Electrostatic Interactions of Peptides with Lipid Membranes: Competitive Binding between Cationic Peptides and Divalent Counterions

by

Roham Rahnamaye Farzami

A thesis
presented to the University of Waterloo
in fulfillment of the
thesis requirement for the degree of
Master of Science
in
Physics

Waterloo, Ontario, Canada, 2010

I hereby declare that I am the sole author of this thesis. This is a true copy of the thesis, including any required final revisions, as accepted by my examiners.

I understand that my thesis may be made electronically available to the public.

Abstract

In this thesis, we investigate a variety of problems involving the interaction of cationic peptides with lipid membranes. To this end we adopt Poisson-Boltzmann (PB) theory and coarse-grained models of these molecules. We first examine the electrostatic interaction of a positively-charged peptide with a negatively charged membrane immersed in a salty solution. In particular, we study how this interaction is influenced by peptides geometry, valence of salt ions, and lipid demixibility. Also we develop a more analytically tractable approach to peptide-membrane association, and then compare it with our PB approach. Finally, we study the interactions of cationic antimicrobial peptides with the outer leaflet of the outer membrane of Gram-negative bacteria. In particular, we incorporate charge discreteness and thus transverse charge correlations on the membrane surface. The main effect of charge discreteness is to enhance the affinity of counterions, especially multivalent ones, for the membrane. This effort enables us to study the competitive binding between cationic peptides and divalent counterions. Our results offer a physical explanation for the observed preferred binding of cationic antimicrobial peptides onto the outer leaflet of Gram-negative bacteria over divalent counterions.

Acknowledgements

I would like to take this opportunity to acknowledge those who have helped me complete this thesis. First and foremost, I would like to express my deepest gratitude to my supervisor, Professor Bae-Yeun Ha – his encouragement, support, and thoughtful advice have been immensely valuable, both in personal and professional terms. I am indebted to him because of his patience with me as well as his generous help throughout my Master's program.

I was honoured to have Professors Z.Y. Jeff Chen, Jamie Forrest, and Hartwig Peemoeller in my advisory and defense committees. Their valuable constructive comments and suggestions helped me a lot to improve the quality of my research as well as this thesis. This thesis would not be possible without their support and encouragement.

I am thankful to Sattar Taheri-Araghi, the senior member of our research group. His constructive pieces of advice helped me a lot to progress in my research projects. I owe him a lot for sharing his valuable experiences with me and helping me throughout all difficulties in my research work.

I owe my parents so much for everything I have earned in my life. Their understanding and support have always encouraged me to be confident and have a strong belief in my dreams. Their passion and enthusiasm have always been the ultimate source of energy for me to not give up during the life difficulties. I also owe one of my very first physics teachers and mentors, Nima Hamedani Radja, who soon became a great friend and colleage of mine. I am thankful to him for showing me how to enjoy science and follow it as a passion.

I have been blessed in my life to be surrounded by amazing friends. In particular, I would like to extend my sincere gratitude to Mani Kashanianfard, Yasaman Amintowlieh, Sharad Birmiwal, Bryan Yeung, and Jillian Sauder because of all their support and encouragement while I was working on this thesis. Their presence changed the frustrating times of writing this thesis to joyful memorable moments.

Last but not least, I am deeply grateful to Erica Robinson who kindly and generously read this thesis and helped me to improve the quality of it by her thoughtful suggestions.

This thesis is dedicated to my parents
for all their support.

Contents

List of Figures

Chapter 1

Introduction

1.1 Cell Membrane and Lipid Bilayer

Cells are the fundamental units of life. The simplest and most ancient types of cells are *prokaryotes*, and these include *bacteria*. Plants, fungi, and animals are collectively called *eykaryotes*. Eukaryotic cells are typically bigger than prokaryotes. In both groups, the cell contents are bound by their plasma membrane that separates the cell's internal components from extracellular materials. The membrane is made of a *lipid bilayer* and membrane-bound proteins. Lipids are *amphipathic* (amphiphilic) molecules, each consisting of separate hydrophobic (nonpolar) and hydrophilic (polar) parts. The hydrophobic part is insoluble in polar solvents (such as water) while the hydrophilic part is soluble. Therefore, in water, these molecules self-assemble into structures such as a closed lipid bilayer so as to hide their hydrophobic part from and expose their hydrophilic part to the water molecules [1].

Most of natural bilayers are composed primarily but not exclusively of a class of lipids called *phospholipids*. The hydrophobic part of a phospholipid consists of two long fatty acid chains ("tails") [see Figure 1.1]. Each fatty acid chain consists of a sequence of carbon atoms with a carboxyl group (–COOH) at the end. Their hydrophilic part (often referred to as the head group) contains a negatively charged phosphate group; a glycerol molecule connects this hydrophilic head group to the hydrophobic tails.

There is usually a *phosphate* ($H_2PO_4^-$) group joined to another head-group molecule such as serine (the resulting lipid is called phosphatidylserine – PS), glycerol (phosphatidylglycerol – PG), coline (phosphatidylcholine – PC), or ethanolamine (phosphatidylethanolamine – PE). Some of these head groups are negatively charged (like PS). Therefore, the lipid bilayers that are comprised of phospholipids can bear a negative charge density. For instance, the inner layer of the plasma membrane of red blood cells, i.e., the membrane

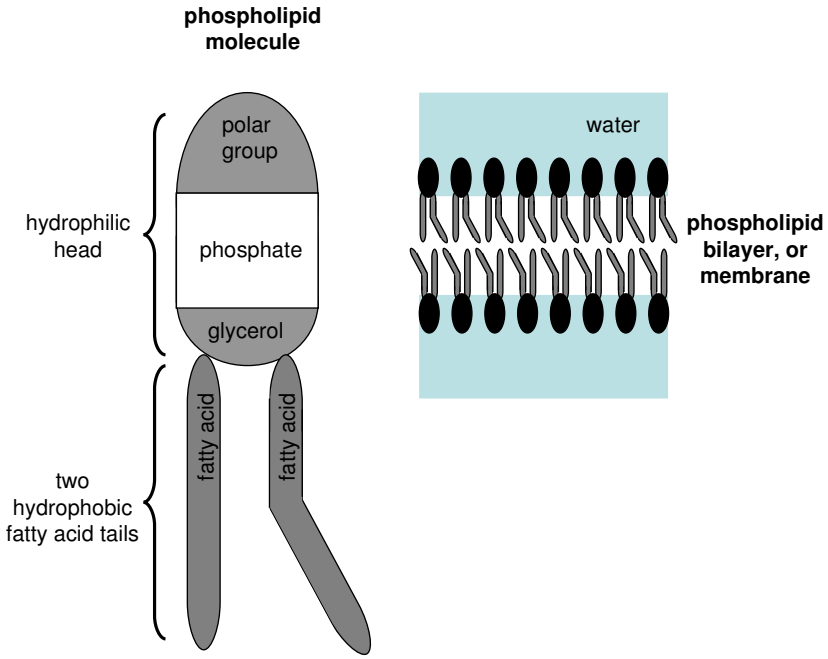

Figure 1.1: Schematic view of a phospholipid and a lipid bilayer. Left: The hydrophobic tails and hydrophilic head of a phospholipid are shown. Note that the entire hydrophilic part is polar and the polar group joined to the phosphate group can be one of molecules such as serine, glycerol, coline, and ethanolamine. Right: Orientation of phospholipids in a bilayer. They are oriented so as to hide their hydrophobic part from and expose their hydrophilic part to surrounding the water.

surrounding the cell, is negatively charged. It is particularly important to note that lipids as well as other macromolecules within the membrane (such as membrane proteins) can more or less freely diffuse laterally in the two-dimensional lipid bilayer, which allows them to respond to interactions with other charged macromolecules.

1.2 Antimicrobial Peptides

Peptides are short polymers formed by a sequence of amino acids. One of the main distinctions between peptides and proteins is that peptides have shorter sequences than proteins. There is a notable group of peptides that show antimicrobial activity against pathogens (i.e., bacteria, viruses, or other microorganisms that could cause disease). These peptides are called *antimicrobial peptides* (AMPs) and are recognized as important components of the innate defence mechanism of multicellullar organisms (i.e., animals and plants). They are also sometimes called "host defence peptides": they exhibit "selective" toxicity against microbes (e.g., bacteria, enveloped viruses, fungi), while leaving the host cells intact [35, 5].

AMPs can be categorized into different subgroups based on their physical structure and characteristics. AMPs are typically 10-45 amino acids long. They can be cationic or anionic, but the cationic ones are more active in binding to microbes, and are therefore of more interest. In this context, AMPs can have a variety of structures. However, they usually adopt an amphiphilic structure with α-helical or β-sheet shapes when bound to a membrane (Figure 1.2).

Antimicrobial activity and specificity of AMPs can be affected by different physical characteristics [5, 21]. Physical characteristics of AMPs, such as size, sequence, charge, structure, hydrophobicity, and amphipathicity can determine their affinity for a lipid membrane and thus their biological activity (e.g., membrane permeabilization). While there is extensive empirical studies on how peptide parameters can play a role in the activity of AMPs [8, 18, 7, 34], a quantitative picture of the physical mechanism that underlies the relationship between peptide parameters and their activity is still elusive [5]. Our theoretical understanding of how peptide parameters may play a role in the activity of AMPs has remained far behind current empirical advances, despite its therapeutic benefits for designing new AMPs.

1.3 Gram-negative Bacteria and LPS Leaflet

Bacteria are one of the three main branches of the tree of life. The others are Archaea and Eucaryotes [1]. Based on shape, bacteria can be classified as rods, spheres, or spirals. They are also classified as either *Gram-positive* or *Gram-negative* based on their so-called

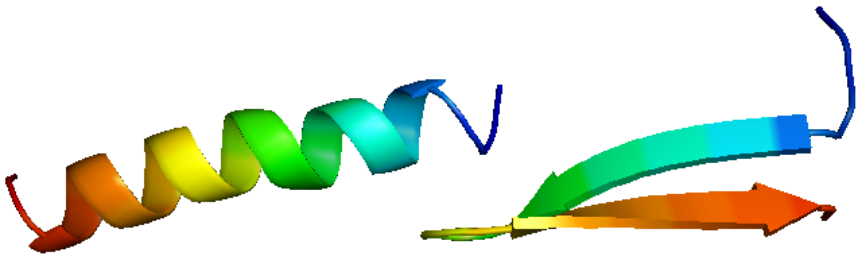

Figure 1.2: Two very common structures of antimicrobial peptides – Left: an α-helical structure, Magainin 2 (PDB code 2mag; GIGKFLHSAKKFGKAFVGEMNS); Right: a β-sheet structure, Protegrin 1 (PDB code 1pg1; RGGRLCYCRRRFCVCVGR). Images generated by using PyMOL and downloading the original PDB files from PDB bank. The letters shown for each peptide are the standard abbreviations for amino acids. See Appendix 1.6.1 for their full name.

Gram-staining property [1]. Gram-positive bacteria have a single membrane and a thick cell wall made of a mesh-like layer of *peptidoglycan*, a polymer consisting of sugars and amino acids. Because of the peptidoglycan layer in Gram-positive bacteria, they retain the violet dye used in the Gram staining procedure and are therefore called Gram-positive. Gram-negative bacteria such as *E. coli* and *Salmonella* have two membranes (see Figure 1.3). Their peptidoglycan layer is located between the two membranes and is thinner than the peptidoglycan layer in Gram-positive bacteria. These bacteria, therefore, fail to retain the dye in the Gram-staining procedure.

The inner membrane of Gram-negative bacteria is a phospholipid bilayer, and the inner leaflet of the outer membrane is also comprised mostly of phospholipids. The outer leaflet of the outer membrane, however, is made of a different kind of lipid called *lipopolysaccharide* (LPS). The outer membrane of Gram-negative bacteria thus has an asymmetric LPS-phospholipid bilayer [27].

LPS is a large molecule consisting of lipid A, an inner and outer core of polysaccharide joined by a covalent bond, and an outermost region of *O*-antigen (Figure 1.4). LPS is considered as a polyanionic lipid – that is, a lipid that consists of a couple of monophosphate and carboxyl groups. In particular, there are usually two monophosphate groups in lipid A as well as a few carboxyl and monophosphate (or diphosphate) groups in the inner core region. Considering that each lipid A molecule has six hydrophobic chains, the density of negative charge per hydrocarbon chain is more than 1. The high concentration of LPS in outer leaflet of the outer membrane of Gram-negative bacteria makes it highly negatively charged. Therefore, the presence of divalent counterions in solution is crucial for charge neutralization, i.e., bridging of negative charges, and therefore for maintaining the stability of the LPS leaflet, which would otherwise be unstable [27]. Studies even show that the

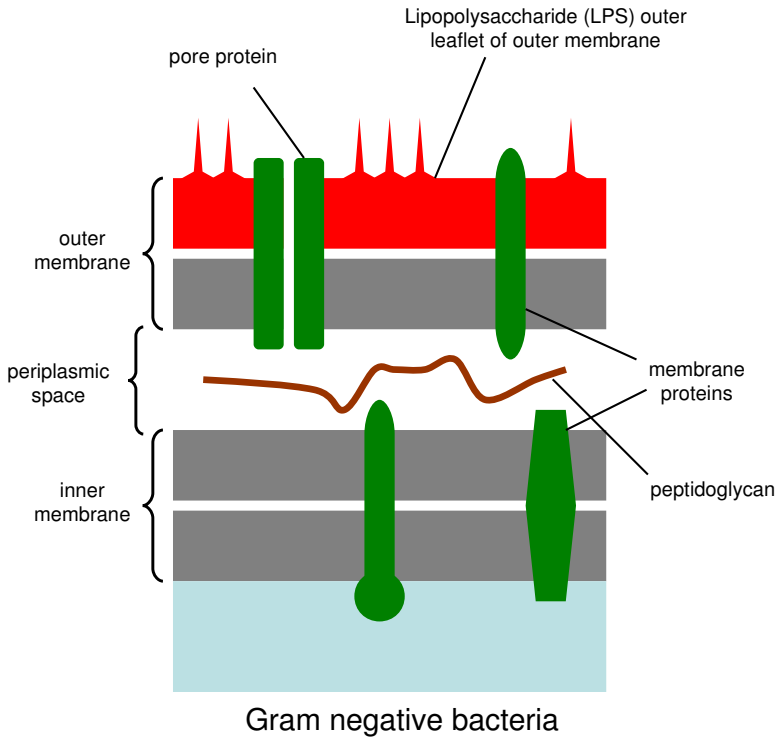

Figure 1.3: Schematic view of a Gram-negative bacteria membrane. From bottom to top: the inner or cytoplasmic membrane consisting of a phopholipid bilayer, the peptidoglycan layer between the two membranes, and the outer membrane whose inner leaflet is primarily made of phospholipids and outer leaflet is composed of LPS molecules.

lateral association of LPS molecules is not possible in the absence of divalent cations [19].

Cationic antimicrobial peptides such as magainin II can attach to and perturb the outer membrane of the Gram-negative bacteria. Despite much experimental progress in this field, a quantitative picture of the mechanism behind this disruption is not yet clear [see Reference [10] and the references therein]. The third chapter of this thesis is an attempt to study the interactions of cationic antimicrobial peptides with the outer leaflet of Gram-negative bacteria, providing a theoretical explanation for their mechanism of action.

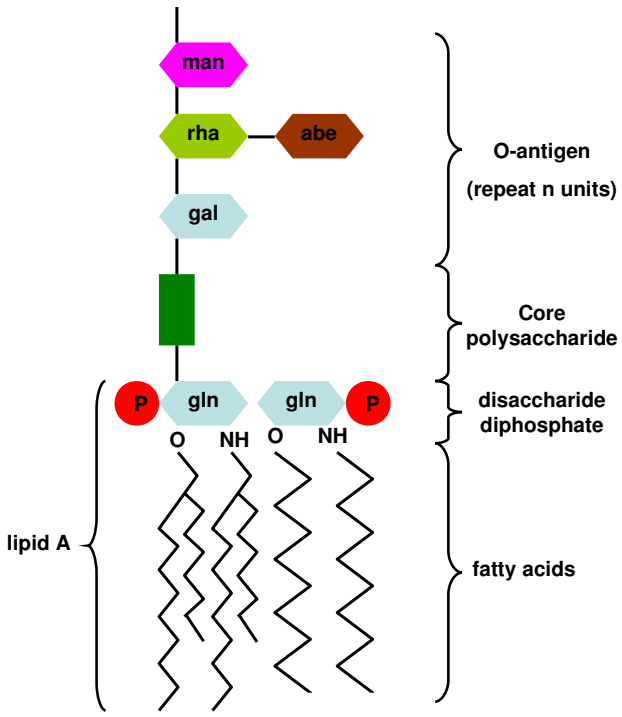

Figure 1.4: Schematic structure of a lipopolysaccharide (LPS) molecule. From top to bottom: O-antigen region (also referred to as polysaccharide) is a polymer of sugar molecules, the core domain which contains an oligosaccharide (sugar) component, and lipid A region consisting of two glucosamine (carbohydrate/sugar) units attached to fatty acids. Normally, there is one phosphate group on each carbohydrate of the Lipid A region.

1.4 Poisson-Boltzmann Theory

Many of the objects in biological systems (i.e., molecules, colloids, polymers, membranes, etc) are at least partially charged, and thereby, can interact electrostatically with other charged objects. However, since these objects are immersed in aqueous media, a systematic consideration of the contribution of mobile ions is key to understanding the electrostatic interactions of macro-molecules.

The Poisson-Boltzmann (PB) approach is a standard theoretical tool for calculating the coulombic potential around charged particles in such media [23, 30]. This approach is mean-field in nature and relies on a couple of assumptions. For example, Coulombic interactions are the only interactions between charged objects and thus other kinds of interactions, such as permanent or induced dipole-dipole interactions, are neglected in the PB approach. Furthermore, the charges are often assumed to be point-like and any

finite size effect is thus neglected. Another assumption is that the aqueous solution is represented by a continuous medium with a uniform dielectric constant ϵ. The electric potential that each ions experiences as well as the charge density of ions in solution are continuous functions.

The PB approach provides a good analytical approximation for many applications. Because of its nonlinear nature (see Eq. 1.3), however, this approach allows a closed-form analytical solution for a limited number of boundary conditions. However, with non-trivial boundary conditions, finding the solutions numerically is inevitable. The PB theory works especially well in physiological conditions (electrolyte strength of about 0.1 M) and/or as long as the surfaces of charged objects are not highly charged. However, due to the mean-field nature of the PB theory, it is not able to completely describe the features of solutions with multivalent salts, though it is reasonably successful in producing good results for monovalent ions.

The PB equation can be constructed as follows: First, Poisson's equation relates ϕ, the electrostatic potential at a given position, to ρ, the charge density at that position. In the SI units, Poisson's equation reads

$$\nabla^2\phi = -4\pi\rho/\epsilon_r \tag{1.1}$$

where ϵ_r is the dielectric constant of the medium. Next, we relate ρ to ϕ. To this end, note that the total charge density at each position $\vec{r}$ is the sum of two ion densities: $\rho(\vec{r}) = ez_+n_+(\vec{r}) + ez_-n_-(\vec{r})$. The ion concentration, n_i, is given by the Boltzmann distribution,

$$n_i = n_i^0 \exp\left(\frac{-z_i e\phi}{k_B T}\right) \tag{1.2}$$

where n_i^0 is the reference density of ion species i (i.e., cations or anions) and z_i is the valence of the ion. Finally, k_B is Boltzmann's constant and T is the temperature.

Combining Equations 1.1 and 1.2, we get the *Poisson-Boltzmann equation*, which self-consistently determines the electric potential in an aqueous solution. It proves useful to introduce the dimensionless potential, $\Psi \equiv e\phi/k_BT$, and to recast the PB equation as:

$$\nabla^2\Psi = -4\pi l_B \sum_i z_i n_i^0 e^{-z_i\Psi} \tag{1.3}$$

where $l_B = e^2/(\epsilon_r k_B T)$ is known as the Bjerrum length. For a solution with added 1:1 and 2:1 salts, by using the electroneutrality condition $\sum_i z_i n_i^0 = 0$, the PB equation becomes

$$\nabla^2\Psi = 8\pi l_B n_1^0 \sinh\Psi + 8\pi l_B n_2^0 (e^{\Psi} - e^{-2\Psi}) \tag{1.4}$$

and the density of monovalent and z-valent ions can be derived from

$$\begin{aligned} n_{-1} &= z n_0 e^{\Psi} \\ n_{+z} &= n_0 e^{-z\Psi} \end{aligned} \tag{1.5}$$

For such a solution with added 1:1 and Z:1 salts, Debye-Hückel screening length, κ^{-1}, is given by the relation $\kappa^2 = 4\pi l_B[2n_1^0 + Z(Z+1)n_2^0]$.

1.5 Overview of the thesis

In chapter 2 of this thesis, we re-examine the interaction of cationic peptides with a demixable lipid membrane. We study in detail the energetic and entropic contributions of the free energy of such a system. Using the mean-field Poisson-Boltzmann (PB) theory for ions near charged surfaces, we develop a detailed physical picture of how the counterion release process governs the peptide-membrane interaction. Based on this detailed physical picture, we study how peptide-membrane parameters influence the interaction. In particular, we focus on how and to what extent such factors as peptide geometry, the valence of salt ions in solution, and demixability of lipids in the membrane may change our understanding about this interaction. Then, we develop a coarse-grained semi-analytical approach to calculating the binding energy of a thin peptide and a lipid membrane, and, finally, we compare the results of semi-analytical calculations with numerical results.

In the last chapter, we study the interactions of cationic antimicrobial peptides with the outer leaflet of the outer membrane of Gram-negative bacteria. To encapsulate the effect of charge correlations, we use a simple model which allows ions to bind locally to discrete surface charges. The charge correlation effect is shown to enhance counterion condensation on the membrane. Importantly, this approach enables us to study the competitive binding of cationic peptides and divalent ions to a lipid membrane. Our results suggest a physical explanation for the preferred binding of (moderately to highly charged) cationic antimicrobial peptides on the outer leaflet of Gram-negative bacteria over divalent counterions.

1.6 Appendices

1.6.1 Amino acids and their short symbols

Alanine	A
Arginine	R
Asparagine	N
Aspartic acid	D
Cysteine	C
Glutamic acid	E
Glutamine	Q
Glycine	G
Histidine	H
Isoleucine	I
Leucine	L
Lysine	K
Methionine	M
Phenylalanine	F
Proline	P
Serine	S
Threonine	T
Tryptophan	W
Tyrosine	Y
Valine	V

Chapter 2

Electrostatic Interaction Between a Model Peptide and a Membrane

2.1 Introduction

A variety of processes in biological systems are driven or affected by electrostatic interactions [12]. Examples include DNA packing, the selective activity of antimicrobial peptides, and the bending of asymmetrically-charged membranes. In all of such processes, the coulomb interaction between charged biomolecules is influenced by the ambient salt ions. Along this line, much research has been focused on determining the role of salt ions. While in simple terms, salt ions merely screen and reduce the strength of coulomb interactions, some exotic effects, driven by salt ions, have been observed in biological systems. Perhaps, the most well-known effect is attraction of like-charged surfaces mediated by multivalent counterions – the physical basis of DNA packing in viruses (DNAs are negatively charged).

Theoretical research over the last few decades has revealed the details of the electrostatic interactions in a salty solution (see References [2, 12, 22, 29, 31]). A simple, yet very informative, example is the interaction between two oppositely charged plates. The expectation is that they would always attract. However, depending on the magnitude of charges on each plate, their interaction can change into repulsion at short distances depending on whether energy or entropy dominates (a detailed review of this system is presented in the next section). While the electrostatic energy prefers all charges to collapse to a single point, entropy, on the other hand, prefers an even ion distribution throughout the system. Presence of geometrical constraints, such as shape and deformation of a biomolecule, as well as the valence of ions can complicate the system.

In this chapter, we study the electrostatic interaction between oppositely charged objects. First, we review the problem of oppositely charged plates and explain the interactions

as a balance between the energy and the entropy of the system. We then move to models with more biological relevance: a charged disk and cylinder interacting with an oppositely charged surface. These latter cases can be used for the modelling of the interaction of charged peptides or proteins with cell membranes.

The strength of our analysis relies on the explicit analysis of different factors contributing to the free energy, relating them to the release of counterions. That is, upon binding of oppositely charged objects, their counterions (oppositely charged ions with respect to their binding object), which are previously trapped in the vicinity of the object, can leave the interaction zone and gain entropy. We also examine the subtle effect of charged-lipid demixing and the resulting modulation of surface charges as it happens on biological membranes.

2.2 Theory

In this section, we present a theory for studying the electrostatic interaction of charged macromolecules in ionic solutions. We calculate the free energy for a system consisting of two charged parallel plates, and then we extend the theory to calculate a more geometrically complicated system with more biological relevance.

2.2.1 Two charged parallel plates

We begin by studying the interaction between oppositely charged objects by analyzing the electrostatic interaction between two charged plates. As we discussed in the introduction, the Poisson-Boltzmann (PB) approach provides a powerful analytical tool for studying the electrostatic interactions in electrolytes. The PB equation for a system immersed in a 1:1 (monovalent) ionic solution (*e.g.*, Na^++Cl^-) reads

$$\nabla^2\Psi = \kappa^2 \sinh(\Psi), \tag{2.1}$$

where $\Psi = e\phi/k_BT$ is the dimensionless potential with e the electronic charge, ϕ the electrostatic potential, and k_BT the Boltzmann constant. Finally, κ is the inverse Debye screening length defined by $\kappa^2 = 8\pi l_B n_0$, where n_0 is the bulk concentration of monovalent ions, and $l_B = e^2/\epsilon k_BT$ is the Bjerrum length with ϵ the dielectric constant. At room temperature, $l_B \simeq 7$Å in water where $\epsilon \simeq 80$.

The differential equation 2.1 should be solved with proper boundary conditions based on the geometry of the charged objects. The boundary conditions for two oppositely charged semi-infinite flat surfaces in the (x, y) plane with a uniform charge density $\sigma_\pm$ located at

$z = \pm h/2$ is given by

$$\left.\frac{d\Psi}{dz}\right|_{z=\pm h/2} = 4\pi l_B \sigma_{\pm}, \tag{2.2}$$

where $\sigma_{\pm}$ is the planar charge density in units of e. The derivative of the potential with respect to z gives the normal component of the electric field. Given this boundary condition, no electric field penetrates beyond the space defined by two plates. The consistency of this can be confirmed by considering a cylindrical Gaussian surface, which is oriented along the z axis and whose flat side is outside the space between the surfaces. While the electroneutrality condition ensures that the total electric charge of the system is zero, Gauss' law demands that the electric field should vanish outside the space defined by the two surfaces.

Once the Poisson-Boltzmann equation is solved subject to the boundary conditions, one can proceed to calculate the free energy of the system. Knowing $\Psi(\mathbf{r})$, the dimensionless local electrostatic potential, the free energy of the system can be written as:

$$F = \frac{1}{8\pi l_B}\int (\nabla\Psi)^2 d\mathbf{r} + \int \left[n_+ \ln\left(\frac{n_+}{n_0}\right) + n_- \ln\left(\frac{n_-}{n_0}\right) - (n_+ + n_- - 2n_0)\right] d\mathbf{r}, \tag{2.3}$$

where the first term accounts for the electrostatic energy of the system, and the second term is the translational entropy of salt ions, with n_i being the concentration of the ith ion species at $\mathbf{r}$ and, n_0 the bulk concentration of ions where the potential is zero. These two integrals run over the whole space between the two charged plates. Therefore, the electrostatic free energy is computed by plugging in the solution of the PB equation (Equation 1.3) into Equation 2.3, and carrying out the integral over the whole space.

2.2.2 A charged disk or a cylinder near a surface

In this section, we present some models related to biological systems. In the past, spherical and disk models have been used for charged proteins and peptides interacting with cell membranes. For the computational purpose, a hexagonal arrangement was assumed for bound molecules [22, 31] – each bound molecule thus defines a 'Wigner-Seitz' (WS) cell. With this simplification, binding free energy and the density of bound molecules were then calculated. Here, we compare disk and cylinder shaped charged objects interacting with charged membranes. These geometries are inspired by previous theoretical models as well as by antimicrobial peptides that adopt α-helical structure near cell membranes.

In our model, the circular disk is considered to have diameter of 20Å and thickness of 8Å so that its cross-section and volume correspond to that of typical antimicrobial peptides (AMPs). Also, we assume that one half of the peptide has a positive charge, Q (in units of the elementary charge e). Following References [31, 18], we opted for $Q = 4$ for the peptide

charge, as it is a typical value for peptides such as magainin 2. In order to capture the amphiphilic structure of AMPs, we set the dielectric constant of the charged (i.e., polar or hydrophobic) part to $\epsilon_P = 40$, and the dielectric constant of the upper hydrophobic half to $\epsilon_H = 3$. For the peptide modelled as a cylinder, we assume a diameter of 10Å and length of 10Å. The dielectric constant of the peptide is chosen to be 40. The membrane is modelled as a sheet with the thickness of 40Å and dielectric constant of $\epsilon_l = 2$, immersed in a Z:1 electrolyte solution. To mimic the charged properties of lipid bilayers, we assume the outer layer of the membrane consists of zwitterionic (neutral) and anionic lipids with a headgroup area of $a_0 = 65\text{Å}^2$. The fraction of anionic lipids at each point, $\alpha(x, y)$, determines the surface charge density of the outer layer of the membrane, i.e., $\sigma(x, y) = -e/a_0 \times \alpha(x, y)$. We shall consider two cases of membranes, one with a uniform charge distribution and the other with demixable anionic lipids. The latter means that anionic lipids can move to the interaction zone if an oppositely charged molecule approaches the membrane.

The total free energy of one peptide (a disk or a cylinder in our model) and a membrane can be written as:

$$\begin{aligned} F =& \frac{1}{8\pi l_B} \int (\nabla\Psi)^2 d\mathbf{r} + \int \left[n_+ \ln\left(\frac{n_+}{n_0}\right) + n_- \ln\left(\frac{n_-}{n_0}\right) - (n_+ + n_- - 2n_0) \right] d\mathbf{r} \\ &+ \int \left[\alpha \ln\left(\frac{\alpha}{\bar{\alpha}}\right) + (1-\alpha) \ln\left(\frac{1-\alpha}{1-\bar{\alpha}}\right) \right] \frac{d\mathbf{r}_\perp}{a_0} + \lambda \int (\alpha - \bar{\alpha}) \frac{d\mathbf{r}_\perp}{a_0} \end{aligned} \tag{2.4}$$

where $\mathbf{r}_\perp = (x, y)$. Here, the first term accounts for the electrostatic energy of the system, including contributions from charges both on the surface and in bulk; the second term describes the translational entropy of salt ions as influenced by the peptide and anionic lipids in the WS cell; and the third term takes into account the entropy of redistribution of anionic lipids. The last term guarantees the total charge conservation on the outer layer of the membrane; the Lagrange multiplier λ has to be adjusted such that the last integral vanishes. In the case of no lipid demixing, the last two terms do not contribute to the free energy.

The equilibrium condition of a system can be determined by minimizing its free energy. To minimize the free energy functional in equation 2.4, the Poisson-Boltzmann (PB) equation has to be solved subject to the boundary conditions. The minimization of Equation 2.4 with respect to $\alpha(\mathbf{r})$ results in [31, 22],

$$\alpha(\mathbf{r}) = \frac{\exp(\Psi(\mathbf{r}) - \lambda)}{(1-\bar{\alpha})/\bar{\alpha} + \exp(\Psi(\mathbf{r}) - \lambda)} \tag{2.5}$$

In fact, equation 2.5 works as a boundary condition of a demixable charged lipid membrane, and the PB equation should be solved self-consistently with this and other boundary conditions.

2.3 Results and Discussions

In this section, we present our results with an emphasis on how the competition between energy and entropy controls the electrostatic interactions between charged objects. We first discuss the interactions between two planar surfaces and then move on to look at more geometrically complicated systems with more biological relevance.

2.3.1 Two oppositely charged surfaces

In the case of two uniformly and asymmetrically charged planar surfaces (Figure 2.1), the electrostatic interaction between the surfaces can be either attractive or repulsive depending on the surface charge densities and their separation. Appendix 2.4.1 2.4.2 presents a general argument about the sign of interaction for two arbitrarily charged surfaces (also, see References [24, 12]). For a large separation, each surface is completely screened by the counterions in solution. As a result, the electrostatic potential around each plate decays to zero due to the cloud of counterions accumulating in the vicinity of the charged surface. If $|\sigma_+| = |\sigma_-|$, the interaction between the surfaces always is attractive. This is mainly because of the entropic gain of released counterions. That is, as the two surfaces get closer to each other, equal numbers of bound counterions are paired up and released to the solution, while electroneutrality is retained. This process is accompanied by a gain in the entropy, which is favourable. However, if there is a charge mismatch (i.e., $|\sigma_+| < |\sigma_-|$), some counterions are trapped in the proximity of the charged surfaces to neutralize the existing excess backbone charges of the surfaces. The residual counterions trapped between the plates resist further confinement, and thus make the interaction repulsive when the surfaces are in close proximity. Note that this repulsion will not always occur if the counterions are allowed to move behind the charged surfaces, which is possible, but not the case in our model.

Using the theoretical framework presented in the previous section for two charged parallel plates, we will solve the PB equation (Equation 1.4) with proper boundary conditions for two uniformly charged planar surfaces. We will use the solution to calculate the free energy of the system, as well as the total number of salt ions released from and remaining within the gap between the surfaces (Figure 2.2).

Figure 2.2 depicts the results of our calculations for the following three cases of two asymmetrically charged surfaces: *i*) both surfaces are exactly oppositely charged ($\sigma_+ = -\sigma_-$) (red lines in the figure); *ii*) one of the surfaces is charged while the other one is neutral (blue lines in the figure); and, *iii*) one of the surfaces bear half charge density of the other one in magnitude (green lines in the figure). Our results are consistent with previous observations and illuminate the role of energy and entropy separately. The top

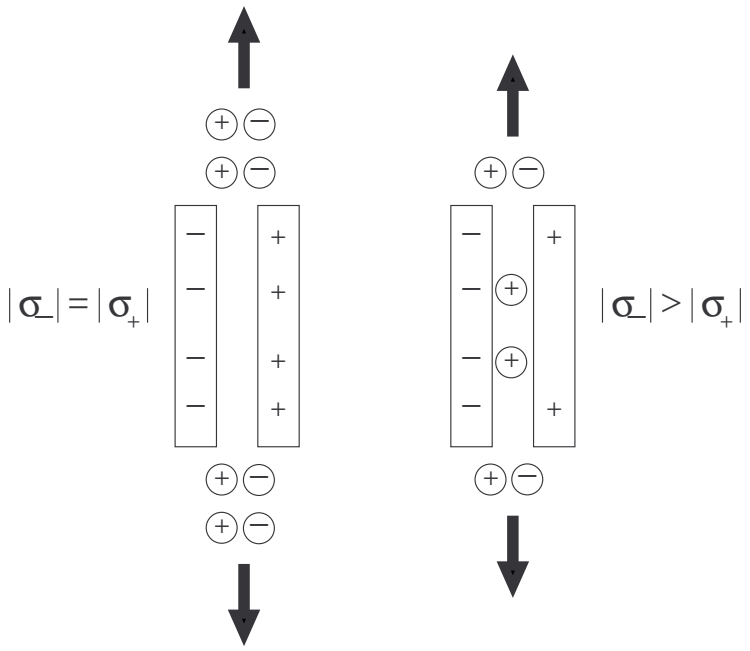

Figure 2.1: (Schematics) Behaviour of counterions near charged surfaces. For two oppositely charged surfaces (left figure), the oppositely charged counterions around them can pair up together and leave the vicinity of the charged surfaces. For the case $|\sigma_-| \neq |\sigma_+|$ (i.e., there is a mismatch in the surface charges) (right figure), some of the counterions remain in the gap between the surfaces in order to neutralize the charge mismatch, turning the attraction into a repulsion at short separations.

panel shows the electrostatic energy of a two plate system as a function of their separation. The middle panel shows the entropic free energy and the bottom panel depicts the total free energy as a function of plate separation. While each curve shows the corresponding (free) energy, the slope of the curves illustrates the force arising from this corresponding energy. In each case, attraction is dominated by an entropy increase that is logarithmically dependent on salt concentration (for a detailed analytical calculation, see Appendix 2.4.1).

The interaction of two oppositely charged surfaces ($\sigma_+ = -\sigma_-$) is always attractive due to the counterion release process (see the red curve in the bottom panel, Figure 2.2). As the two surfaces are brought into close proximity, a proportional number of counterions are no longer required to neutralize the charged surfaces and are freed into the solution. The more the diffusive layers of two surfaces overlap, the more oppositely charged counterions can pair up together and leave the charged surfaces while the electroneutrality condition is maintained. The values on the y-axis of three panels reveal that the main driving mechanism behind the binding process is the entropy gain due to the release of counterions.

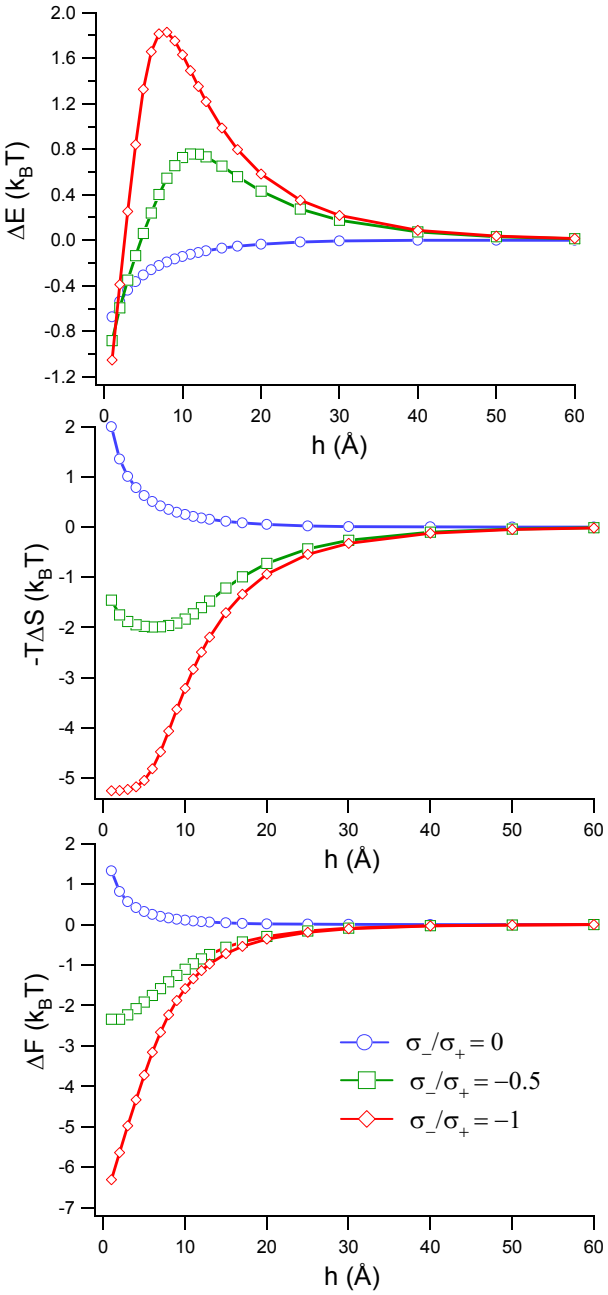

Figure 2.2: Electrostatic interaction of two asymmetrically charged surfaces: a few free energy contributions (per lipid with headgroup area $a_0 = 65\text{Å}^2$): (top) energy (ΔE), (middle) entropy ($-T\Delta S$), and (bottom) free energy term (ΔF) as a function of surface-to-surface separation (h). Three cases for the ratio of surface charge densities (σ_-/σ_+) are plotted: when both surface charges are completely antisymmetric (red triangles), when one of the surfaces bears half charge density of the other one (green squares), and when one of the surfaces is neutral and the other one is charged (blue circles). In this plot, $\sigma_+ = 0.0154$ corresponding to $\bar{\alpha} = 1$.

The entropic gain of released counterions can be understood using the following simple analytical argument: The total gain for the entropic part of free energy is $\simeq -2 \times k_B T \ln[\sigma/(l \times n_0)]$, where $\sigma = |\sigma_\pm|$ and l is a typical length proportional to the ratio of occupied volume of the counterions in bulk rather than on the surface to a_0, $l \sim v_0/a_0$ (see Appendix 2.4.1) with a_0 the typical lipid headgroup area of a lipid (assuming the plates bear charges in the same order as lipid bilayers in biological systems). If we set $l \sim \sqrt{a_0}$, the entropic gain in a 1:1 salt solution with the Debye length $\kappa^{-1} = 10$Å and surface charge density $\sigma = 1/65\text{Å}^{-2}$ is $-7.01 k_B T$. This crude estimate compares favourably with the red curve in middle panel in Figure 2.2, which indicates the entropic gain is equal to $-5.25 k_B T$. The total number of counterion pairs that can be released is proportional to σ, the surface charge density of the surfaces (see section 2.3.2 for a more detailed discussion).

Our results depicted in the top panel in Figure 2.2, show that the electrostatic energy of a two plate system changes non-monotonically as the separation between surface changes. This can be explained using a capacitor analogy, because a charged plate and its diffusive layer can be approximated as a capacitor. The maximum change in the energy of the system owing to release of all counterions trapped in the bilayer is proportional to $\sigma A/2$ (see Appendix 2.4.1). With small separations between the charged surfaces, the screening counterion clouds around the surfaces vanish because of the release of the counterions. The vanishing of the screening clouds allows the backbone charges of the two oppositely charged surfaces to directly interact. In the absence of the screening counterion clouds, the magnitude of the attractive force between the bare charges of the surfaces can become quite significant. Because the diffusive layer capacitor's plates have lost counterions, the energy of the bare charges is more negative than the energy change in the capacitor. Therefore, the non-monotonic energy term is the result of two competing effects: the release of counterion pairs from the gap makes the energy less negative in competition to the direct interaction of backbone charges which causes a more negative energy.

The extent of counterion release depends on the surface charge ratio, σ_-/σ_+. When the surfaces are completely antisymmetric, all the counterions around them are released to the reservoir when two plates are brought close to each other (red curve in middle panel, Figure 2.2), whereas with a neutral and a charged surface, the counterion release never actually happens (blue curve in middle panel, Figure 2.2). In fact, in the latter case, as the separation between the surfaces decreases, the counterion cloud in the vicinity of the charged surface becomes compressed, and as a result, the entropy of ions decreases (i.e., the entropic part of the free energy increases). In such cases, this rise in the entropic part of the free energy is usually expressed in terms of *osmotic pressure*. The osmotic pressure is proportional to the concentration of crowded counterions within the gap between the surfaces. In the case of a neutral and a charged surface, the electroneutrality condition requires that the concentration of crowded counterions in the vicinity of charged surface is proportional to σ; Therefore, the osmotic pressure is $n_\perp k_B T \sim \sigma k_B T$, where $n_\perp$ is the

concentration of counterions in the vicinity of the charged surfaces, k_B is the Boltzmann's constant, and T is the temperature.

In the case of a neutral and a charged surface, the energy of the system monotonically decreases as the separation h decreases (blue curve in top panel, Figure 2.2). The reason is that the trapped counterions in the vicinity of the charged surface are squeezed (both together and to the surfaces) as the surfaces brought close to each other. This can be explained using a simple capacitor model, where the charged surface and the diffusive layer are the two plates of the hypothetical capacitor. With such a capacitor, the energy decreases as the distance between the plates of the capacitor decreases. As we shall see in more detail in the section 2.3.2, by reducing the separation between two surfaces, some loosely bound counterions have to completely condense on the charged membrane in order to maintain the electroneutrality condition. Therefore, a more accurate model for calculating the energy of such a system would be to imagine a hypothetical capacitor in which the charge on its plates decreases as the plates are brought closer to each other.

2.3.2 Quantifying counterion release effect

As discussed earlier in this section, the entropic and energetic terms that determine the free energy of a charged system in an electrolyte are very closely related to the counterion density and the release of counterions as oppositely charged particles interact. Therefore, it proves useful to measure the number of counterions released from and remaining in the interaction zone for a two plate system. We show in this section that although the counterion release effect is well-understood in the context of the electrostatic interaction between charged objects in the aqueous media, the way it is usually introduced in the literature can be somewhat misleading and confusing in practice. In this section, we refine the definition of the parameter describing the counterion release process (Figure 2.3).

In the literature, the parameter that is commonly used to describe the release of counterions is defined as [2],

$$\eta = \int_{\Omega} \left[2n_0 - n_+(\mathbf{r}) - n_-(\mathbf{r})\right] d\mathbf{r}, \tag{2.6}$$

where the integral carries over the region Ω, the entire separation between the charged objects as well as the areas around the objects. In this equation, $n_\pm$ is the concentration of cations and anions, and n_0 is the bulk concentration of salt ions in reservoir (i.e., where the electrostatic potential is zero). The integration carries over all the volume between the surfaces. Therefore, the parameter η, measures the excess number of charges within the entire gap. The change of this quantity as a function of surface-to-surface separation is plotted in Figure 2.3, left panel. The red and green curves in the figure show that the η decreases as the separation between the plates becomes smaller. This is evidence that

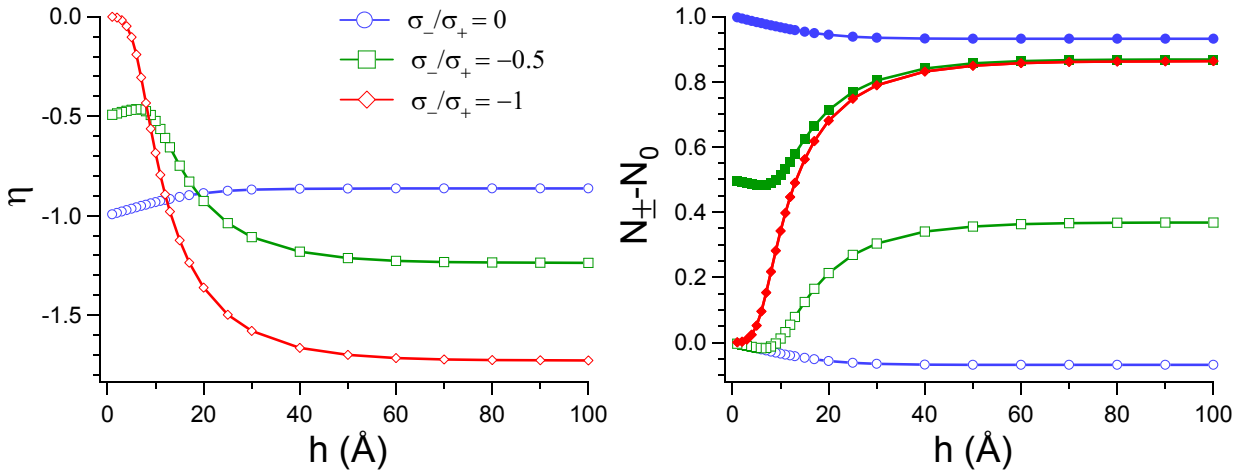

Figure 2.3: Comparison of different possible parameters to present the counterion release process. Left panel: Parameter $\eta = 2N_0 - N_+ - N_-$ as defined in the literature. Right panel: The excess number of anions, $N_- - N_0$, (filled points) and cations, $N_+ - N_0$, (unfilled points). In this plot, $\sigma_+ = 0.0154$ corresponding to $\bar{\alpha} = 1$, and all counterion release parameters are calculated per backbone (surface) charge.

counterions are released. The confusion cause by the standard description of the counterion release process is illustrated by the blue curve, which shows the quantity η increases as the separation gets smaller. This seems to suggest that more ions are trapped in the gap when h is small. However, considering the entropic penalty for confinement of these ions and considering the fact that the system was already neutralized for large h, this is clearly not a correct interpretation of η. We explain this below by breaking η into various components.

If we count the total number of positive (negative) counterions between the surfaces,

$$N_\pm = \int_\Omega n_\pm(\mathbf{r}) d\mathbf{r}, \tag{2.7}$$

the parameter η can be simplified as $\eta = 2N_0 - N_+ - N_-$, where $2N_0$ is the total number of salt ions in the gap if surface charges are turned off. The right panel in Figure 2.3 depicts the excess number of cations (anions), $N_+ - N_0$ ($N_- - N_0$), within the gap as a function of the surface-to-surface separation.

The right panel in Figure 2.3 clearly shows what happens during the counterion release process. For completely antisymmetrically charged surfaces (red curve), there is an equal number of cations and anions within the gap. Each charged plate attracts some counterions to its vicinity. As a result, $(N_\pm - N_0)$ is positive and, as dictated by symmetry, is the same for cations and anions. As the distance between surfaces, h, decreases, oppositely charged counterions pair up and are released into the reservoir. This process continues

until no excess counterions are left within the gap. That is, N_+, N_-, and N_0 all vanish, with the distance going to zero. With a positively charged and a neutral surface (blue curves), however, a number of anions (filled blue symbols) remain in the gap, and there is a deficiency in the number of cations (unfilled blue symbols). These are evident in the fact that the corresponding curves for anions and cations are below one and below zero, respectively, for the whole range of separations between surfaces, h, plotted. This observation suggests that the electroneutrality condition is provided for by both attraction of counterions and repulsion of co-ions. Along this line, the difference between the two blue curves shows the net charge due to salt ions neutralizing the backbone charge. The figure shows that this difference is always one, confirming that one backbone charge is neutralized by salt ions. As the surfaces come close to each other, all to counterions leave the interaction zone and, thus, each backbone charge is neutralized by one counterion. This is shown in the way the blue curve with filled symbol tends to 1 as h goes to zero.

From this analysis, it is clear that the parameter $N_\pm - N_0$ is a better measure of counterion release than the previously used parameter η (Equation 2.6). Indeed, this parameter helps us to better understand the change in the entropic and energetic parts of the free energy, which is an important step toward developing a better picture about the electrostatic interaction between charged surfaces.

2.3.3 A disk or a cylinder interacting with a membrane

In this section we present our results for models with more biological relevance. The models we discuss here have been used in the literature to discuss charged proteins and peptides interacting with cell membranes. Since these interactions are derived from electrostatic interactions, it is worthwhile to study the details of such interactions and their dependence on the geometry of the charged objects.

Here, we choose two different geometries for a model peptide and compare their electrostatic interaction with an oppositely charged membrane. These geometries are *i*) a thick disk partitioned in two halves and *ii*) a cylinder parallel to the membrane, as illustrated in Figure 2.5. The first geometry is used in the literature mainly because of its rotational symmetry. That is, if there are multiple peptides bound to the surface, their symmetry can force them to form a hexagonal lattice on the surface. In this case, each ligand defines a WS (Wigner-Seitz) cell such that the total free energy of the system can be calculated based on this cell's energy. The thick disk partitioned into two halves is inspired by amphipathic peptides where the two sides of a folded molecule have different charge and hydrophobic properties. The second geometry, i.e. the cylindrical peptide, is inspired by alpha-helical structure of peptides which tends to align parallel to the membrane.

The membrane is a sheet with thickness 40Å and dielectric constant $\epsilon_l = 2$ immersed

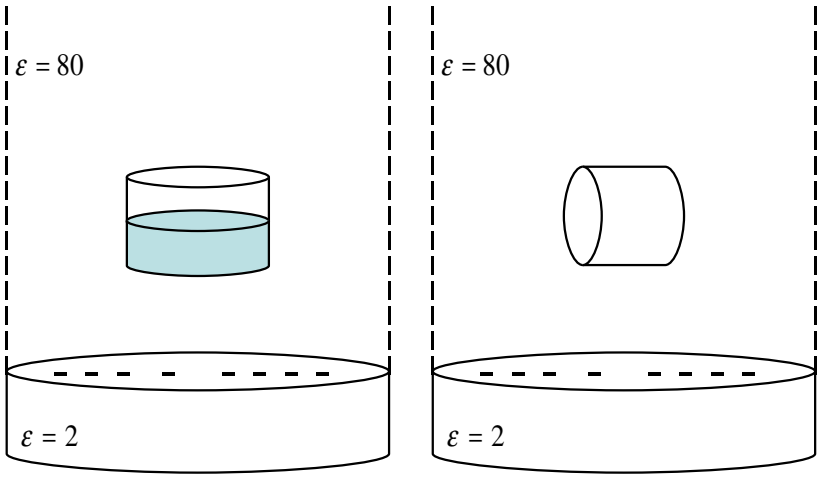

Figure 2.4: Schematic view of different geometries of a model peptide and a model membrane – the model peptide is chosen to be (left) a thick disk and (right) a cylinder. The model membrane is a sheet with a dielectric constant $\epsilon = 2$, immersed in an electrolyte with dielectric constant $\epsilon = 80$.

in a 1:1 or 2:1 electrolyte. The outer layer of the membrane consists of zwitterionononic and anionic lipids with constant optimal headgroup area $a_0 = 65\text{Å}^2$.

For a peptide modelled as a thick disk, we assume a diameter of 20Å and thickness of 8Å. The two halves present the hydrophobic and hydrophilic parts of an amphipathic peptide with dielectric constants of 3 and 40, respectively. The hydrophobic part has a positive charge Q. For a peptide modelled as a cylinder, we assume a diameter of 10Å and length of 10Å. The dielectric constant of the peptide is chosen equal to 40. For both cases, the peptides bear a positive charge of $Q = +4$, the typical charge value for AMP.

Based on what we discussed in section 2.3.1, we can extend the general picture for the interaction of two asymmetrically charged surfaces to these model peptides with a membrane. In Figure 2.5, we compare the parameters defining the interaction of our model peptides with a membrane, as a function of peptide-membrane separation. As can be seen in the plots, the peptide-membrane interaction is qualitatively similar for different peptide shapes.

As described in detail in the section 2.3.1, the counterion release process, and thus the entropic free energy, is the driving mechansim behind the binding of charged macromolecules. As depicted in the middle panel in Figure 2.5, the difference in the entropic free energy between our disc and cylinder models is smaller than k_BT and is even less significant for more weakly charged lipid membranes. One point to note is that, with the values we chose for the charges of the peptide and membrane, the opposite surface charges

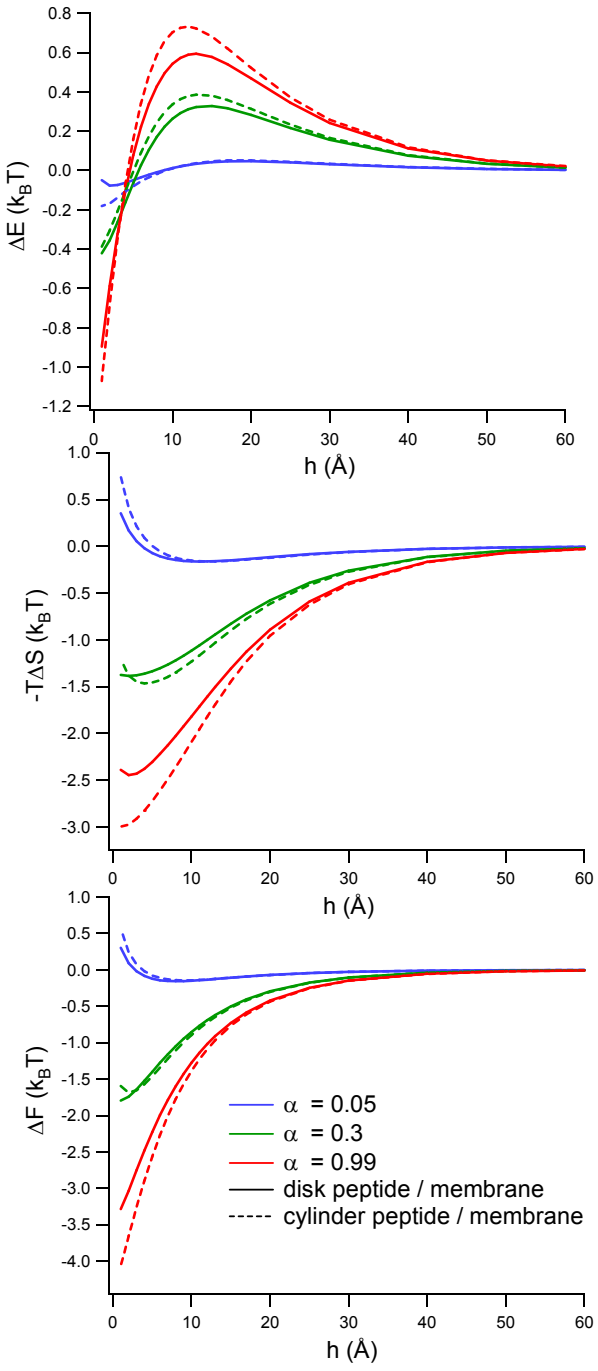

Figure 2.5: Effect of the peptide's geometry on the interaction of a model peptide with a model membrane. A few free energy contributions (per lipid with headgroup area $a_0 = 65$Å) are plotted as a function of the peptide-membrane distance for a thick disk peptide (solid lines) and a cylinder peptide (dotted line) interacting with a model membrane. The membrane's surface charge density is assumed to be uniform and constant.

of the peptide and membrane can almost match in magnitude. Because of this, they can gain the highest possible amount of counterion release (the red curves in the middle panel of Figure 2.5).

2.3.4 Effect of multivalent counterions

The PB theory is a mean-field theory, and therefore neglects the effect of short-range charge correlations between free and/or bound ions. These inter-ion charge correlations become important, especially when the surfaces are strongly charged and the solution contains an enough concentration of multi-valent ions. In chapter 3 of this thesis, we show that these charge correlations play a major role in the overcharging of the membrane or other macromolecules [12]. We shall show that these short-range charge correlations affect the interaction of the charged macromolecules with their surrounding ions and charged objects. In this sense, the PB theory is not able to provide a satisfactory and complete picture of the electrostatic interactions of the divalent ions. However, this theory has proven to be quite useful in describing the coulombic interactions between charged macromolecules, especially in the case that objects are not highly charged.

In order to further elaborate on the mechanism we described in the previous sections, we study the effect of valence of the released counterions on the free energy terms of a peptide-membrane system. This study also provides us with a numerical support for the simple analytical calculations we presented in Appendix 2.4.1.

Figure 2.6 compares the free energy terms of a system of peptide-membrane in the presence of monovalent or divalent counterions. As can be seen, both the energy and entropic terms of the free energy diminish in magnitude in the presence of divalent counterions. In the presence of divalent salt, a smaller number of (divalent) counterions are needed to neutralize the anionic lipid membrane. As a result, a smaller amount of counterions are released for the same peptide-membrane separation (the red curves in the middle panel of Figure 2.6). In addition, along with what we predict based on the counterion release mechanism, the decrease in free energy terms becomes larger in magnitude (i.e. by a couple of k_BT) for membranes with a higher fraction of anionic lipids because more condensed counterions exist in the vicinity of highly charged membranes, and therefore, more counterions can be released by approaching peptides.

The top panel in Fig 2.6 shows that the height of the hump in the energy plot decreases in the presence of divalent salt. This result is understandable in light of our earlier explanation for the nature of this nonmonotonic change. As described in section 2.3.1, this hump is the result of the competition between two effects: the release of counterion pair makes the energy term less negative while the direct interaction of unscreened oppositely charged surfaces makes the energy more negative. As mentioned, in the presence of di-

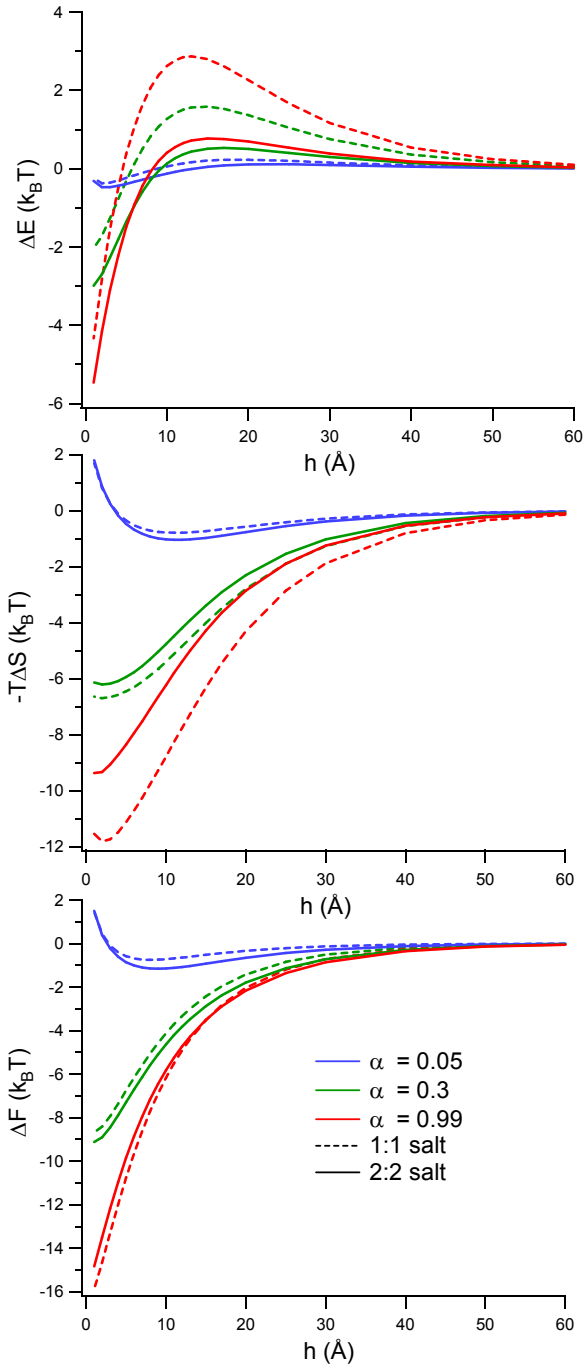

Figure 2.6: Effect of multivalent counterions on the interaction between a peptide and a membrane. Various free energy contributions (per lipid), i.e., (top) energy, (middle) entropy, (bottom) free energy, are shown as a function of membrane-to-peptide separation (h). Comparison of the two cases: added 1:1 (monovalent) salt (dotted lines) and added 2:2 (divalent) salt (solid lines). The lipid membrane is assumed to be non-demixable.

valent counterions in the solution, a thinner counterion cloud exists around the charged objects, and therefore, fewer counterion pairs are released from charged macromolecules.

2.3.5 Effect of lipid demixability

The surface charge density of biological lipid membranes is not constant and fluctuates within the surface of the membrane. This fluctuation exists because biological membranes often carry a binary fluid mixture of monovalent acidic (negatively charged) lipids and zwitterionic (electrically neutral) ones. In the absence of charged macromolecules, this mixture is uniformly mixed. Upon binding of charged macromolecules (in our model, the cationic peptides) onto the bilayer, the anionic lipids can accumulate in the immediate vicinity of the adsorbed peptide, and thus, redistribute (i.e. demix) themselves such that the density of negatively charged lipids increases near the guest, i.e., the positively charged peptide. This migration of anionic lipids toward the adsorbed macromolecule helps the membrane to achieve the electroneutrality condition locally, and as a result, lowers the electrostatic energy of the system. The redistribution of anionic lipids triggered by peripheral macromolecules, however, may involve an unfavourable entropic penalty [22, 20, 9].

In this section, we study in detail how demixability of membrane lipids can influence the electrostatic interaction between a model peptide and a membrane. Figure 2.7 shows the influence of lipid demixability on the free energy of the system as the demixing is turned 'on' and 'off'. As expected and clearly depicted in the middle panel in Figure 2.7, the effect of demixability of lipids is noticeable on the entropic free energy (see the solid and dotted lines for the blue and red curves in the middle panel). The effect of demixing can be seen as an unfavourable entropic penalty which increases at small separations in the peptide-membrane system. This entropic penalty is more pronounced as the anionic lipids in the membrane have more freedom to redistribute themselves (the blue curve with $\bar{\alpha} = 0.05$ in the middle panel). In this case, the electrostatic interaction can even become repulsive for small separations of the peptide and membrane (the blue curve in the bottom panel). However, the demixing entropy penalty is quite negligible in the case of an almost fully charged membrane, because the redistribution of anionic lipids changes the charge profile little (the red curve with $\bar{\alpha} = 0.99$ in the middle panel).

In line with the previous findings in the literature, the magnitude of the binding free energy of a non-demixable membrane is significantly smaller than that of a demixable membrane [see blue and red curves in bottom panel in Figure 2.7]. This happens because the free energy gain increases when lipid mobility is permitted as anionic lipids gather around the bound peptide in order to satisfy charge matching. This process, however, will cause release of some confined counterions into the bulk solution.

As shown in the bottom panel, local demixing of anionic lipids in the vicinity of adsorbing macromolecules can result in significant enhancement of the free energy. This is

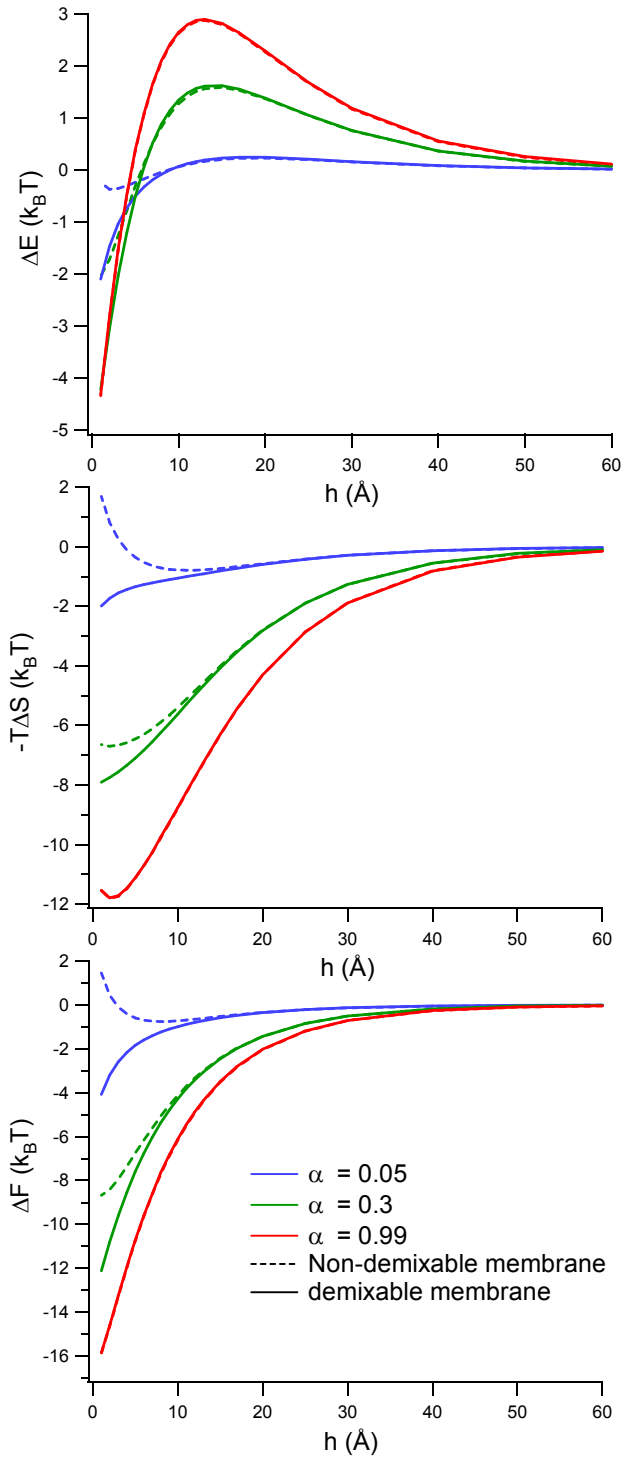

Figure 2.7: Effect of lipid demixability on the interaction between a peptide and a membrane. Free energy as a function of peptide-membrane distance for non-demixable (dotted line) and demixable (solid line) lipid membrane in the presence of a 1:1 salt solution with Debye length $\kappa^{-1} = 10$Å.

particularly true for the lower surface charge densities of the membrane (i.e. blue curves with $\bar{\alpha} = 0.05$) for which the charge mismatch between the peptide and membrane at the point of contact is substantial. For such a case, the adsorption free energy change can be as large as $\sim 6\ k_B T$.

2.3.6 Equilibrium adsorption concentration: Semi-analytical calculations

In this section we develop a coarse-grained semi-analytical approach to calculating the binding energy of a thin peptide and a lipid membrane. More specifically, we find an analytical tractable model for computing the free energy of a Wigner-Seitz cell of radius A_{WS}, as a function of its radius and peptide-membrane parameters.

The peptide is a thin disk with area A_p and charge of Q. Our approach can be extended to account for other geometries when the thickness is suppressed. The membrane is, as in previous sections, assumed to be made of neutral and charged lipids with $\overline{\alpha}$ being the average fraction of charged lipids. The membrane and lipids are immersed in a (1:1) salt solution with the inverse Debye length κ.

Our approach is based on the solution of one dimensional Poisson-Boltzmann equation. Following Reference [15], the electrostatic energy and free energy of a charged surface immersed in a (1:1) salt can be derived analytically. A mean-field approach to peptide binding assumes that all peptide charges are smeared out on the surface. The net charge density reads $\sigma_{net} = -e\overline{\alpha}/a_0 + Q\sigma_p$. One can use this net surface charge to calculate the free energy of binding. The main drawback of this approach is that it underestimates the effect of the charge correlations, which in this case occurs mainly through the demixing of charged lipids. Charge correlations increase the binding energy and trigger more peptide binding.

In the approach developed here, we take into account the demixing of lipids in a non-trivial way and calculate the free energy of a WS cell. That is, the membrane surface is divided into two main zones: 1) zone with a peptide and surrounding (with total area A_s); 2) bare membrane, as illustrated in the Figure 2.8. The fraction of charged lipids in zone 1 and 2 are not the same and are found by minimization of the free energy subject to the constraint that the total number of lipids is conserved. To find the free energy of the WS cell, zones 1 and 2 are treated separately. This is obviously a nontrivial approximation and its accuracy can be checked *a posteriori*. The average charge densities (in units of e) are $\sigma_1 = Q/A_s - \alpha_1/a_0$ and $\sigma_2 = -\alpha_2/a_0$ for zones 1 and 2, respectively. Following Reference [15] the free energy of each part per unit area is:

$$\mathcal{F}_{el}(\sigma, \kappa, \ell_B) = \sigma\Psi_0 - \frac{\kappa}{\pi\ell_B}\left[\cosh\left(\frac{\Psi_0}{2}\right)\right] \tag{2.8}$$

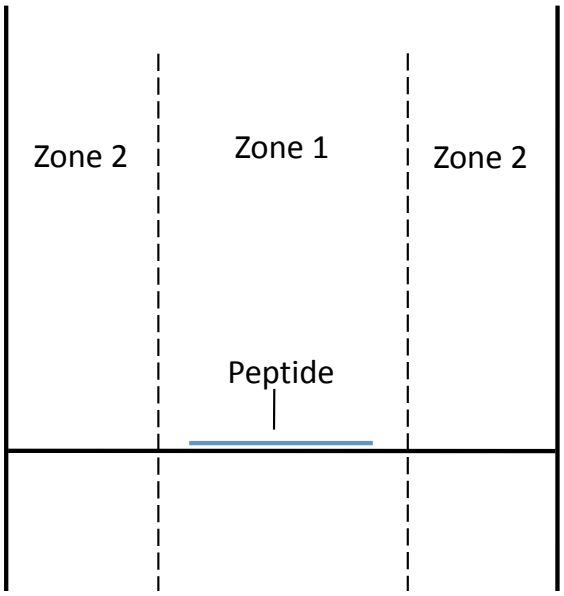

Figure 2.8: Schematic view of zones 1 and 2 with a bound peptide for the semi-analytical calculations. Zone 1 consists of a bound peptide and its surrounding anionic lipids and zone 2 represents the bare membrane. We assume that the fraction of charged lipids in zones 2 is higher than that in zone 1 because more anionic lipids tend to accumulate around the cationic bound peptide. In our calculations, we assumed that the radius of zone 1 is equal to the two-dimensional Debye screening length.

with Ψ_0 the electrostatic potential on the surface given by,

$$\Psi_0 = 2\sinh^{-1}(2\pi\sigma\ell_B/\kappa). \tag{2.9}$$

The total free energy of the WS cell can be calculated as:

$$F_{\rm WS} = A_s\mathcal{F}_{el}(\sigma_1,\kappa,\ell_B) + (A_{\rm WS} - A_s)\mathcal{F}_{el}(\sigma_2,\kappa,\ell_B) \tag{2.10}$$

There is an ambiguity in defining the area of the zone 1, A_s. In principle, A_s includes the peptide area as well as the area surrounding the peptide in which lipids effectively interact with the peptide. What is this extended area? To answer this question, we use the two-dimensional Debye screening length, κ_2^{-1}, introduced by Velazquez and Blum [33]. Based on their theory, only lipids within this screening length interact with the peptide. For a disk peptide with area $A_p = \pi R_p^2$, we can define the interaction zone area by $A_s = \pi(R_p + \kappa_2^{-1})$, where $\kappa_2 = 2\pi e^2\overline{\alpha}/(a_0\epsilon k_B T)$ for a membrane with $\overline{\alpha}$ the average fraction of charged lipids and a_0 the head group area of lipid molecules.

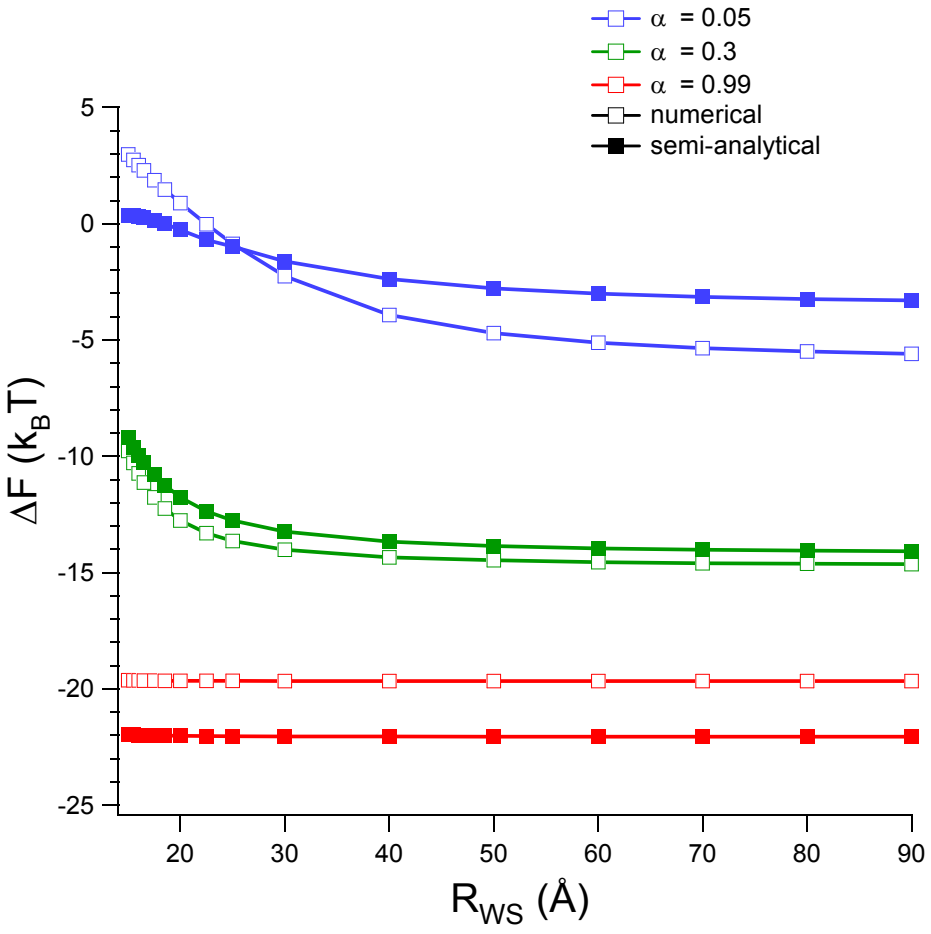

Figure 2.9: Adsorption free energy of an infinitely thin model disk peptide onto a demixable membrane as a function of the WS cell radius. Comparison of results of numerical solution and semi-analytical calculations.

In this section, we compare our numerical results with the semi-analytical approach we presented. Within the Wigner-Seitz picture, the concentration of bound peptide to the membrane can be determined by minimizing the adsorption free energy with respect to the WS cell's radius. Figure 2.9 shows the adsorption free energy of a model peptide into a demixable membrane as a function of the WS cell radius for both monovalent and divalent salt.

Our numerical results (curves with unfilled squares in Figure 2.9) show that as the number of peptides adsorbed onto the membrane increases, they compete in recruiting the charged lipids into their vicinity. The adsorption free energy changes more non-monotonically as a function of the cell radius R_{WS} for the lower values of $\bar{\alpha}$ (the average fraction of anionic lipids) because the lower values allow the competitive recruitment of

anionic lipids to proceed to a greater extent. As explained in previous sections, this recruitment of anionic lipids restores electroneutrality locally around the binding zone. However, the gain in electrostatic energy by the stronger binding is significantly compensated for by the entropy loss caused by the migration of anionic lipids into vicinity of bound peptides.

Figure 2.9 also depicts the difference between the numerical and semi-analytical calculations. It illustrates that for a mid-range value for a membrane charge density (i.e. $\bar{\alpha} = 0.3$), which is more common in the natural bilayers, the semi-analytical calculation is in good agreement with the numerical results. However, for very low or very high membrane charge densities, the semi-analytical calculations deviate from the numerical results. The reason is that for those values of $\bar{\alpha}$, our approximation for finding the the two-dimensional Debye screening length as well as the interaction zone area, A_s, becomes poor.

2.3.7 Summary and Conclusion

To summarize, we reconsidered and elaborated on a simple description of the interaction of a model peptide with a lipid membrane. Using the Poisson-Boltzmann theory, we calculated the free energy terms as a function of peptide-to-membrane separation, and then articulated the relationship between the free energy terms and the physical picture with which the counterion release process provides us. We further showed that the counterion release process can be understood more clearly if someone calculates the number of anions and cation in the region between charged surfaces. That being said, we showed that the counterion release process is capable of adequately describing the electrostatic interaction of such systems. We also showed that two oppositely charged surfaces can be used as a good approximation for a system of peptide and membrane interacting electrostatically. In other words, the geometry of the model peptide does not qualitatively change the physical description of the interaction. Furthermore, we studied the effect of the valence of salt ions as well as demixability of lipids on the electrostatic interaction between a model peptide and a membrane. For the multivalent case, the number of released counterions is reduced compared to the corresponding monovalent cases. This effect diminishes the electrostatic interaction between charge macromolecules in electrolytes. We also showed that demixability of lipids can significantly enhance the free energy of the interaction, especially for the lower surface charge densities of the membrane.

We also developed a coarse-grained semi-analytical approach to the binding energy of a thin peptide and a lipid membrane, and then compared the results of our calculations with numerical results. Our semi-analytical calculation is in good agreement with our numerical results, especially for the values of charge densities that are more common in natural membranes.

One may consider studying more complicated geometries for a model peptide and further investigate how the geometry of a peptide can play a role in its electrostatic interaction with a membrane. Our calculations can also be extended to the analysis of peptides with different distribution of hydrophobic and hydrophilic parts, which in turn may provide a better picture about how the amphipathicity of peptides can control their electrostatic interactions with lipid membranes.

2.4 Appendices

2.4.1 Free energy terms of a system in a multivalent salt

In general, for multivalent salt solution, the energetic and entropic terms can be calculated as follows:

For a negatively charge surface, it is plausible to assume that the surface is neutralized by Z valence counterions. We can think of this condensed counterion cloud as a capacitor with planar plates at distance l_{GC} [24]. The electrostatic energy stored in this capacitor is $E = Q^2/2C$, in which Q is the total charge of membrane (equal to the total charge of condensed counterions) and $C = \epsilon A/l_{GC}$, the capacitance of this capacitor. Substituting Gouy-Chapman length for a Z-valency solution, $l_{GC} = (2\pi l_B \sigma_+ Z)^{-1}$, the stored electrostatic energy per $k_B T(= \beta^{-1})$ per unit area, A, is $\frac{\beta E_1}{A} = N_{bb}/Z$. Adding the stored electrostatic energy of both neutralized plates (one with Z-multivalent counterions and the other with monovalent counterions) and choosing the energy reference when the distance between plates is zero, the adsorption electrostatic energy of two antisymmetric surfaces is

$$\frac{\beta \Delta E}{N_{bb}.A} = -\left(1 + \frac{1}{Z}\right) \tag{2.11}$$

The entropy change for $+Z$ valency counterions is

$$\Delta S_Z = \frac{N_{bb}}{Z} \ln(\frac{n_-}{Z} v_0) - \frac{N_{bb}}{Z} \ln(\frac{\sigma_-}{Z} a_0) \tag{2.12}$$

where a_0 is the size of counterions used as lipid headgruop size and v_0 is the space that each counterion occupies. Thus, the total entropic contribution in adsorption of two antisymmetrically charged membranes per surfaces backbone charges is

$$\frac{\beta \Delta F_{ent}}{N_{bb}} = -\left(1 + \frac{1}{Z}\right) \ln(\frac{\sigma_- a_0}{n_- v_0}) \tag{2.13}$$

Since the number of cationic counterion released is N_{bb}/Z, where N_{bb} is the number of backbone charges on the surface, the total number of counterions released per number of backbone charges simply is

$$\frac{\eta}{N_{bb}} = -\left(1 + \frac{1}{Z}\right) \tag{2.14}$$

2.4.2 Sign of interaction for two arbitrarily charged surfaces

Here, following the arguments introduced in References [24, 12], we show that the surfaces bearing charges of the same sign always repel each other, while the interaction between the charged surfaces of opposite signs can be either attractive or repulsive depending on the charge ratio of the surfaces.

We consider two planar surfaces bearing arbitrary surface charge densities separated by a distance h (see Fig 2.10). We assume that space between the surfaces is filled with 1:1

salt solution, and therefore, we can write the PB equation for such a system. Rewriting Equation 2.1 in one dimension and integrating it once gives

$$\frac{1}{2}\left(\frac{d\Psi}{dz}\right)^2 = \kappa^2 \cosh\Psi + C, \tag{2.15}$$

where C is a constant of integration. By re-arranging the terms in equation 2.15, the constant of integration gives the pressure. For a fixed separation h, this pressure (force per unit area) is constant in the entire region between the charged surfaces because the system is in thermodynamic equilibrium. Therefore, the pressure difference between any point in the solution and a reference point of a reservoir where the electrostatic potential and electric field are zero (i.e., bulk concentration equal to n_0), is

$$P = -\frac{1}{8\pi l_B}\left(\frac{d\Psi}{dz}\right)^2 + 2n_0(\cosh\Psi - 1). \tag{2.16}$$

The first term in equation 2.16 is the Maxwell electric field stress tensor (which is equal to the electrostatic energy per unit volume). The second term is the osmotic pressure, which can be calculated from the translational entropy of the ions (similarly to the ideal-gas translational entropy). Note that in equation 2.16, the reference pressure is equal to $2n_0$.

Depending on the sign of the charged surfaces, the sign of the pressure can be either positive (repulsive interaction) or negative (attractive interaction). The first term in equation 2.16 is always less than or equal to zero, while the second one is always greater than or equal to zero. In the case of symmetrically charged surfaces, the sum of these two terms is always positive because the electric field, $d\Psi/dz$, must become equal to zero somewhere between the surfaces, and therefore, $P \geq 0$. (Remember that the pressure is constant in the entire region). In the case of two asymmetrically charged surfaces, however, the electric field is not necessarily equal to zero. For example, if $\sigma_- = -\sigma_+$, at the midpoint, $z = 0$, the electric potential vanishes, but the electric field is non-zero; in this case, $P \leq 0$. However, if for example, the ratio $|\sigma_-|/|\sigma_+|$ is negligible, the electric field close to the neutral surface vanishes, and thus $P \geq 0$.

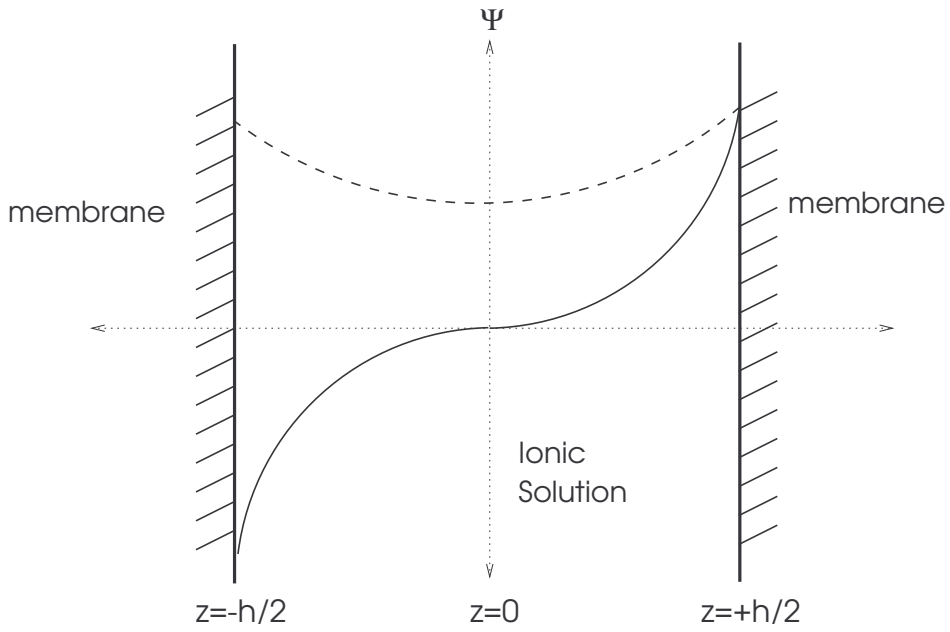

Figure 2.10: Schematic view of two parallel planar surfaces separated by distance h. It shows typical potential profiles for two oppositely charged (solid line) and similarly charged (dashed line) surfaces .

Chapter 3

Competitive Binding between Divalent Ions and Cationic Peptides

3.1 Introduction

Gram-negative (GN) bacteria contain LPS molecules in the outer leaflet of their outer membrane [1]. The LPS molecules are negatively charged and make the outer leaflet of the outer membrane of Gram-negative bacteria highly-negatively charged. One could argue that this high charge density of the outer leaflet makes the bilayer unstable. However, in reality, the outer membrane of Gram-negative bacteria stays stable under the right conditions. The literature shows that bound divalent cations are responsible for holding the outer membrane leaflet structure together [13, 14].

It is well-known that Gram-negative bacteria are ideal targets for the cationic peptides to bind to [27, 10]. Many studies have reported on the interactions between LPS molecules of the GN bacteria's membrane and the cationic antimicrobial peptides, such as magainin, cecropin, and plymyxin. It is believed that electrostatic interactions, which become effective over relatively long distances, play a key role in the binding of the cationic peptides to the outer membrane of the Gram-negative bacteria.

A related phenomenon is overcharging. Overcharging is the extra condensation of counterions onto the surface even after complete neutralization of the charged surface. It is well-known that overcharging occurs in the presence of multivalent ions. Previous studies clearly show that overcharging is not caused by counterion release (which we extensively studied in the previous chapter as the driving force for binding of cationic peptides onto anionic lipid membranes), but rather by the effect of short-range correlations between the ions (at high ion densities). Some analytical approaches have been developed to capture the effects of these short-range correlations especially among multivalent ions [13, 26, 32].

This work is aimed at understanding the interactions of cationic antimicrobial peptides with the outer leaflet of the outer membrane of Gram-negative bacteria, i.e., the LPS layer. Following the approach presented in Reference [16], we use a simplistic model to incorporate transverse charge correlations into the condensation of multivalent counterions on the membrane. First, we show how much the introduced charge correlation can contribute to enhanced condensation of counterions, and therefore, to the overcharging of the membrane. Then, we explore how this model can distinguish between different types of salt ions of same valence (such as Mg^{2+} and Ca^{2+}). Finally, we extend the approach so as to study the competitive binding between cationic peptides and Ca^{2+} ions onto the membrane. In particular, we examine how the preferential binding of cationic peptides displacesdivalent counterions trapped near the LPS layer, as the bulk peptide concentration increases. We shall not, however, consider the formation of pores on the bilayer.

3.2 Theoretical Model

In this section, we first calculate the free energy of a membrane with discrete backbone charges to which multivalent counterions and peptides can bind. Then, by balancing their chemical potentials, we find the equilibrium concentrations of condensed counterions and peptides. To make our physical model biologically relevant, we choose parameter values carefully (see below).

3.2.1 Free energy calculation

Following the approach used in Reference [16], we consider the membrane as a thin flat surface immersed in a solution with added 1:1 salt (such as NaCl) and 2:1 salt (such as $MgCl_2$ or $CaCl_2$). We consider a two-state model – that is, the counterions are either free in bulk or bound to the membrane.

We begin by writing the energy of such a system in the discrete limit. We assume that the membrane is a square lattice with the lattice constant a, and N_s discrete monovalent charges (in units of e), Q_0, are uniformly placed at the nodes of the lattice. These discrete monovalent charges represent the backbone charges of the membrane, and as a result, are the potential binding sites for counterions and peptides. We let N_ν cations with charge (in units of e) Q_ν bind to the binding sites, where subscripts $\nu = 1$ and 2 refer to the monovalent and divalent counterions, respectively. For the sake of simplicity, at this stage in the calculations, we do not consider binding of cationic peptides onto the binding sites; however, our approach can easily be extended to peptide binding. In the discrete limit,

the electrostatic energy of such lattice with its bound cations can be written as

$$\begin{aligned}\beta U =& \frac{1}{2}\sum_{i}^{N_s}\sum_{j\neq i}^{N_s} Q_0 Q_0 u_{ij} \\ &+ \sum_{\nu}\Big(-\sum_{i}^{N_\nu} Q_0 Q_\nu \frac{l_B}{\delta_\nu} - \sum_{i}^{N_\nu}\sum_{j\neq i}^{N_s} Q_\nu Q_0 u_{ij} + \frac{1}{2}\sum_{i}^{N_\nu}\sum_{j\neq i}^{N_\nu} Q_\nu Q_\nu u_{ij}\Big) \\ &+ \sum_{i}^{N_1}\sum_{j\neq i}^{N_2} Q_1 Q_2 u_{ij}, \end{aligned} \tag{3.1}$$

where i and j indicate different binding sites (nodes) on the lattice, and u_{ij} is the electrostatic interaction between two binding sites on the lattice,

$$u_{ij} = l_B \frac{e^{-\kappa|r_{ij}|}}{|r_{ij}|}, \tag{3.2}$$

where $l_B = e^2/\epsilon k_B T$ is the Bjerrum length, ϵ is the dielectric constant of the aqueous media, δ_ν is the size of bound counterions, and κ^{-1} is Debye screening length given by $\kappa^2 = 4\pi l_B[2n_1 + Zn_Z(Z+1)]$, where n_1 and n_Z are the bulk concentration of monovalent and Z-valent ions, respectively.

The first sum in Equation 3.1 is the electrostatic interaction among the backbone charges, excluding the self-interaction of each backbone charge (i.e., $j \neq i$). The second term is the pair-binding energy of N_ν cations of type ν bound to the backbone charge. The third term represents the electrostatic interactions of each bound cation with the backbone charges other than its binding one. The fourth and fifth terms indicate the cation-cation interactions with the same or different types, respectively. Note that self-interactions are omitted in the last three terms.

In this model, only the transverse charge correlations (i.e., interactions between bound cations and backbone charges) are included in the energetic term. It is easy to show that for large separations of backbone charges, the lateral interactions (i.e., between each bound cations and the neighbouring backbone charges) can be neglected in comparison to the transverse interactions (see Reference [11] for a detailed discussion).

Now we can extend Equation 3.1 from the discrete to continuous limit and allow the peptides bind onto the surface as well. In the continuous limit, we model the membrane as a thin flat surface in the (x, y) plane with a surface charge density σ_0 (in units of e). Setting σ_ν and σ_p to be the charge densities of condensed counterions and peptides (in units of e), respectively, and Z_ν to be the valence of the counterions ($Z_1 = 1$ and $Z_2 = 2$) and Q the peptide charge (i.e. $Q = 4$ for the well-known peptide magainin 2), the effective

charge density of the surface can be written as

$$\sigma_{eff} = \sigma_0 - \sum_{\nu=1}^{2} Z_\nu \sigma_\nu - Q\sigma_p. \tag{3.3}$$

In the continuous limit, the lattice can be considered as a uniformly charged surface with area A. Note that, in converting all discrete parameters in Equation 3.1 to continuous quantities, we must be careful not to include $i = j$ terms. Therefore, as we shall see, some correction terms should be added to the total energy in order to prevent simultaneous occupation of a single binding site by more than one counterion. These correction terms are crucial in order to avoid the divergence of the self-energy of the binding sites. The energy of the membrane (per unit area) in the continuous limit can be written as

$$\begin{aligned}
\beta U =& \pi l_B \kappa^{-1} \sigma_{eff}^2 \\
&- \frac{l_B}{2}[\sigma_0^2 + (Z_1\sigma_1)^2 + (Z_2\sigma_2)^2]M_1 - l_B Z_1 Z_2 \sigma_1 \sigma_2 M_1 \\
&+ l_B \sigma_1 \frac{-Z_1}{\delta_1} - l_B Z_1 \sigma_1 (-\sigma_0) M_1 \\
&+ l_B \sigma_2 \frac{-Z_2}{\delta_2} - l_B Z_2 \sigma_2 (-\sigma_0) M_1 \\
&+ l_B \sigma_p \frac{-Q}{\delta_p} - l_B \sigma_p (-\sigma_0) M_4 \\
&- \frac{l_B}{2}\sigma_p^2 M_4 - l_B \sigma_1 \sigma_p Q M_1 - l_B \sigma_2 \sigma_p Q M_1,
\end{aligned} \tag{3.4}$$

where M_ν is a multiple integral which runs over the entire surface of the membrane, except within the regions of $R_\nu \in \{|x - x'| < \nu a, |y - y'| < a\}$ which is excluded in order to avoid the interaction of charges within a single binding site (i.e., equivalent to excluding the $i = j$ cases). The integral M_ν is defined as

$$M_\nu = A^{-1} \iint_{R_\nu} d^2r d^2r' \frac{e^{-\kappa|r-r'|}}{|r - r'|}. \tag{3.5}$$

In fact, this multiple integral M_ν describes the electrostatic interaction of smeared out charges of bound counterions and binding sites over a proper number of binding cells, which in our calculations we integrate over 1 or 4 sites (see Figure 3.1).

The first term in Equation (3.4) is the electrostatic energy of a charged surface with the surface charge density σ_{eff} (see Appendix 3.4.1). In order to include the effect of surface charge discontinuity in our model, this first term in Equation (3.4) should be corrected because self-energy of the backbone charges and bound counterions are already included in

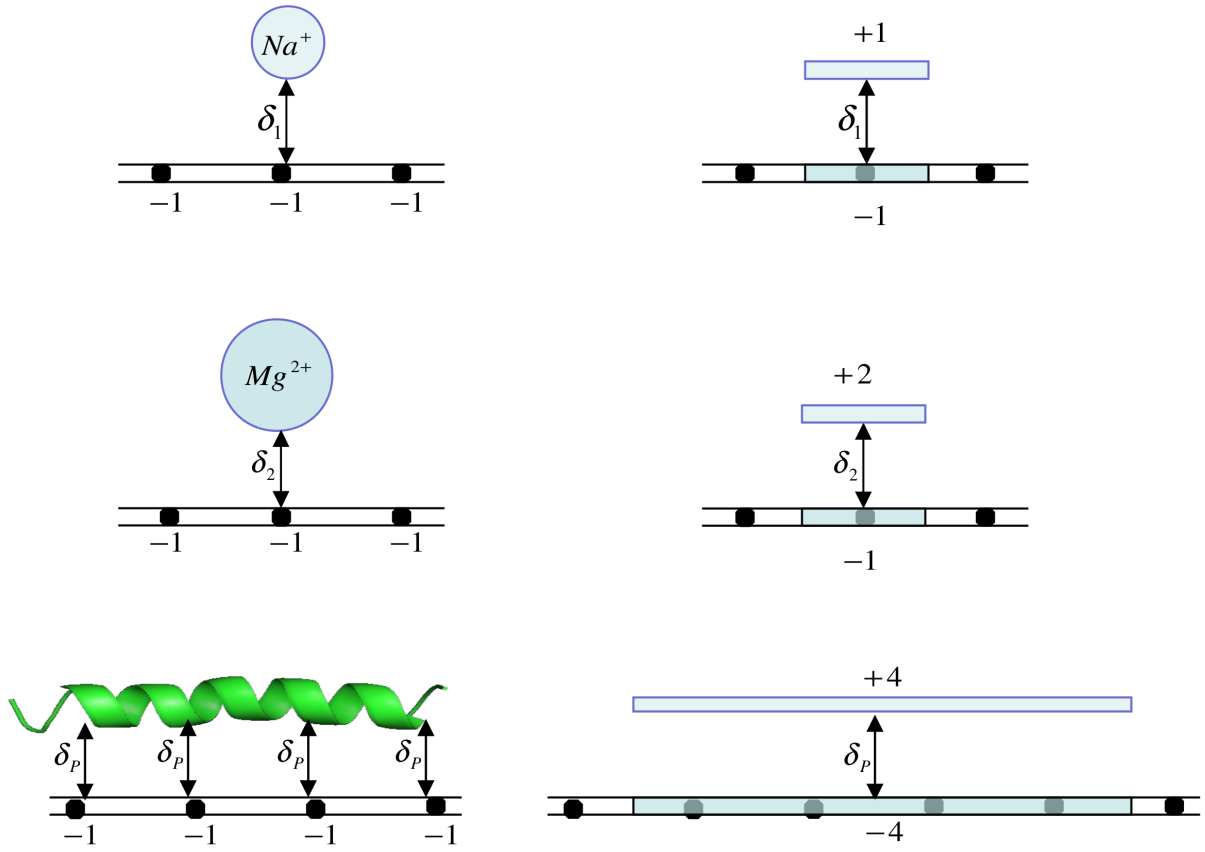

Figure 3.1: Schematic view of the transverse correlations between the bound counterions as well as peptide and discrete backbone charges of the membrane. Each monovalent backbone charge is shown by a black filled circle. The left figures show the location of a bound counterion and peptide relative to the membrane backbone charges, while the right figures show how cationic ions (peptide) are modelled in the mean-field approximation.

this term. The correction terms, therefore, shall run over the entire surface except within the regions of $R \in \{|x - x'| < a, |y - y'| < a\}$ (see Figure 3.1). This constraint ensures that the charge-charge interactions within each site (cell) are excluded in Equation 3.4. Appendix 3.4.2 shows how the multiple integral M_ν is converted to Cartesian coordinates.

The third term in Equation 3.4 shows the pair binding energy created by the interaction of bound counterions with the backbone charge at each binding site. We assume that both bound counterion and backbone charges are point charges and are separated by distance δ_ν from each other. Since these pair binding terms are already taken into account in the first term, we must subtract the continuum limit of each pair binding term using M_ν multiple integral. Therefore, the fourth term can be described as the interaction of each counterion with a smeared out backbone charge over the binding site surface. It is important to note that the absolute value of the third term is greater than that of the fourth term. Using a simple analytical argument, it is easy to show that the integral of the fourth term is proportional to a, the size of lattice constant, and since the membrane's surface charge density is given by $\sigma_0 \sim a^{-2}$, the entire fourth term will be proportional to a^{-1}. In the limit $a \gg \delta$, therefore, the magnitude of the third term in Equation 3.4 becomes greater than its equivalent in the continuum limit. Similarly, the pair binding terms and their correction terms can be written for divalent bound cations as well as bound peptides.

To construct a complete free energy term, we need to include the entropy of the bound counterions on the binding site in the model. The mixing entropy of bound monovalent and divalent counterions on the membrane's surface can easily be calculated using basic statistical mechanics arguments (See Appendix 3.4.3. for a detailed calculation). Note that the size of Mg^{2+} is comparable to that of a backbone charge. Therefore, size-wise, each Mg^{2+} can occupy a space of one backbone charge, but in terms of its charge, each Magnesium ion is able to bind onto two backbone charges. Assuming this, the entropy of Mg^{2+} ions can be written in a similar way to that of Na^+. However, these different ions contribute to the electrostatic energy of the system to different extents.

Therefore, the total free energy of such system per unit area of membrane can be written as

$$\begin{aligned}\beta\mathcal{F} =& \pi l_B \kappa^{-1} \sigma_{eff}^2 - \frac{l_B}{2}\left[\sigma_0^2 + \sum_{i=1}^{2} \sigma_i^2 Z_i^2 - 2\sum_{i=1}^{2} \sigma_i Z_i \sigma_0\right] \int_{-a/\sqrt{2}}^{+a/\sqrt{2}} \int_{-a/\sqrt{2}}^{+a/\sqrt{2}} dX dY \frac{e^{-\kappa\sqrt{X^2+Y^2}}}{\sqrt{X^2+Y^2}} \\ &- \sum_{i=1}^{2} l_B \frac{\sigma_i Z_i^2}{\delta} + \sum_{i=1}^{2} \sigma_i \ln\left(\frac{\sigma_i/\sigma_0}{n_i v_0}\right) + (\sigma_0 - \sigma_1 - \sigma_2)\ln\left(1 - \frac{\sigma_1}{\sigma_0} - \frac{\sigma_2}{\sigma_0}\right) \end{aligned} \tag{3.6}$$

From this, we can calculate the equilibrium concentration of bound counterions by balanc-

ing the chemical potentials of free ($\beta\mu_f^\nu = \ln(n_\nu v_\nu^0)$) and bound species ($\mu_b^\nu = \partial\mathcal{F}_b/\partial\sigma_\nu$):

$$\ln(n_\nu v_\nu^0) = -2\pi l_B \kappa^{-1}\sigma_{eff} Z_\nu - Z_\nu u_b^\nu + l_B \sigma_{eff} M_1 Z_\nu + \ln\left(\frac{\sigma_\nu}{\sigma_0 - \sigma_1 - \sigma_2 - \sigma_p}\right)$$
$$\ln(c_f v_p) = -2\pi l_B \kappa^{-1}\sigma_{eff} Q + l_B \frac{-Q}{\delta_p} + l_B \sigma_{eff} M_1 Z_\nu + \ln\left(\frac{\sigma_\nu}{\sigma_0 - \sigma_1 - \sigma_2 - \sigma_p}\right) \qquad (3.7)$$

where M_ν is the double integral defined in Equation 3.5, and subscripts $\nu = 1, 2$ and p refer to the monovalent counterions, divalent counterions, and peptides, respectively. Therefore, by solving the three nonlinear equations in Equation 3.7 simultaneously, the equilibrium values for σ_1, σ_2, and σ_p can be calculated.

3.2.2 Choosing parameters of the model

In order to utilize our model, we need to choose proper values for the parameters of our model. There is no consensus in the literature about what are accepted values for some of the parameters of our model. We modelled the LPS layer of the Gram-negative bacteria as a square lattice with discrete backbone charges, with the lattice constant parameter to be chosen appropriately. According to experimental work, which analyzed the conformation of LPS molecules in bilayers, the LPS molecules are located in the nodes of a two-dimensional hexagonal lattice (see Reference [27] and the references therein). In our model, we assign one electric charge ($-e$) to each binding charge to mimic each monovalent charged phosphate group in the LPS molecule. Studies show that on average the phosphate groups in LPS molecules are separated from each other by 6 to 8Å [27]. Other studies suggest that the average headgroup area of LPS molecules are around 148Å^2 [28]. Considering that each LPS has 4 mono-charges, the average distance between mono-charges comes close to 6Å. Yet, note that the actual separation between mono-charges is a bit larger than 6Å, because LPS is a bulky molecule and the mono-charges are not located in a single plane. Therefore, based on the proposed conformations for LPS molecules, we will set the value $a = 8$Å for the lattice constant.

Another set of parameters that need be set for our model are the gap sizes between the bound counterions (peptide) and the backbone charges. We should be cautious about choosing the values for the gap sizes, because it turns out that the outcome of our model is sensitive to these values. We used the following criterion for finding the acceptable gap size values. In order to have the model physically meaningful, we require that the value of each correction term in equation 3.4 be less than its corresponding binding term value. This condition gives us the upper boundary for the gap size between the bound counterions and membrane (i.e., $\delta_{1,2} \leq 1/(\sigma_0 M_1)$), and the gap size between the bound peptides and membrane (i.e., $\delta_p \leq Q/(\sigma_0 M_4)$). Therefore, the upper boundaries for the allowed gap

sizes are functions of the bulk concentrations of monovalent and divalent salt ions as well as the lattice constant, a. For the range of added salt concentrations normally used in the experimental studies and according to the lattice constants which we set earlier, the upper boundaries $\delta_{1,2} \leq 1.5$Å and $\delta_p \leq 3.4$Å are acceptable in our model.

We use three types of ions in our model: Na^+, Mg^{2+}, and Ca^{2+}. As we know, for small ions, as well as divalent ions such as Li^+, Be^{2+}, and Mg^{2+} in an aqueous solution, the interaction of dipoles in water molecules with these ions is significant compared to large or monovalent ions. Therefore, the water molecules can make fairly strong bonds with the small or divalent ions. By definition, the *hydration radius* of an ion is the radius of the ion including its tightly-bound water molecules. The hydration radius of an ion is larger than its bare radius (ı.e., its crystal lattice radius). Small ions and highly charged ions are more hydrated and therefore have larger hydrated radii than large and less highly charged ions [17]. Also, note that the cations are typically smaller than the anions of the same valence, because cations lose an electron rather than gaining one; therefore, cations are more hydrated than anions in water, as long as their atomic numbers are similar. Since increasing the valence of the cations can increase the amount of hydration, stable hydration shells (sheaths) can be formed around ions such as Be^{2+} and Mg^{2+}.

Based upon the chemical properties of ions (see the chemical radii in Reference [17]) and the criterion we already set, we choose $\delta_{Na} = 0.95$Å, $\delta_{Ca} = 0.99$Å, $\delta_{Mg} = 1.5$Å, and $\delta_p = 2.3$Å for the gap sizes between the binding sites on the membrane and bound counterions of sodium, calcium, magnesium ions, as well as peptides. Also, the radii of free ions in bulk are chosen equal to $R_{Na} = 3.6$Å, $R_{Ca} = 4.1$Å, and $R_{Mg} = 4.3$Å. The volume of peptide was set equal to 2500Å^3, according to the experimental size of magainin.

3.3 Results and discussions

3.3.1 Charge correlations and membrane overcharging

Studies show that the spatial correlations among charged objects which are ignored in the conventional mean-field theory become important in the presence of multivalent ions in the solution. In fact, many studies show that the spatial correlations among multivalent ions cause overcharging of charged surfaces immersed [3].

Surface overcharging (or charge inversion) occurs when the interfacial charges bind to a number of counterions in excess of the number needed to neutralize their own nominal charge. As such, the net surface charge inverts [26, 11]. In general, two conditions need to be met for a macromolecule to become overcharged. First, the macromolecule should be immersed in a Z:1 salt solution. Different valencies for cations and anions will result

in excess binding of one of them to the charged surface. Note that the overcharging effect can not be observed in the symmetric Z:Z salts because both anions and cations have the same valence and an overcharged surface can adsorb more ions of the opposite sign, which means the surface will always be neutralized. The second condition is that enough divalent salt ions are present in the solution.

It is worth noting that the binding affinity for a membrane is different for monovalent and divalent counterions. In fact, under the right conditions, the divalent ions almost completely replace the monovalent ions bound onto the backbone charges. This is because each divalent ion adsorbed to a backbone charge can take an energy gain larger than k_BT, while the same interaction between a monovalent ion and a backbone charge obtains an energy less than k_BT [26]. Therefore, in the presence of monovalent and divalent salts in the solution, the amount of condensed divalent ions determines the effective charge density of the membrane. Note that the charge inversion occurs because of the finite size of divalent ions bound to each backbone charge in our model and the resulting transverse charge correlations (see Figure 3.1).

In this section, we study the effect of transverse charge correlations (ı.e., the charge correlation between bound ions and surface backbone charges) in the presence of multivalent and monovalent salts. We show that the surface can become overcharged even with a few millimolar concentration of divalent salts.

Figure 3.2 shows the ratio σ^*/σ_0 (ı.e., the ratio of the effective charge of the surface to its bare charge) as a function of the bulk concentration of monovalent ions in the presence of different concentrations of Ca^{2+} ions. We compared the net surface charge density of the membrane obtained from the PB mean-field model, which lacks charge correlations, and our model, which captures transverse charge correlations. As depicted in Figure 3.2, for the mean-field case, the effective surface charge density increases as the concentration of monovalent salt in the solution increases. At the mean-field level, balancing the chemical potentials of bound counterions on the surface and free counterions in bulk gives:

$$-\pi l_B \kappa^{-1} \sigma^* \simeq \ln(n_1 v_0) \tag{3.8}$$

Note that since $n_1 \ll 1$, the result of the logarithm on the right-hand side becomes a finite and negative number. Therefore, according to equation 3.8, we have $\sigma^* \sim \kappa \sim \sqrt{n_1}$, the effective surface charge density of surface should be larger for higher concentrations of monovalent ions, which is in agreement with Figure 3.2.

For the model with added transverse correlations, however, the counterions can condense on the surface. In our our two-state model, counterions can form bonds with backbone charges. As depicted in Figure 3.2, for enough concentration of Ca^{2+} and in the presence of charge correlations, charge inversion occurs. This finding is in line with existing results [3]. Interestingly, the charge inversion is highly sensitive to the presence of

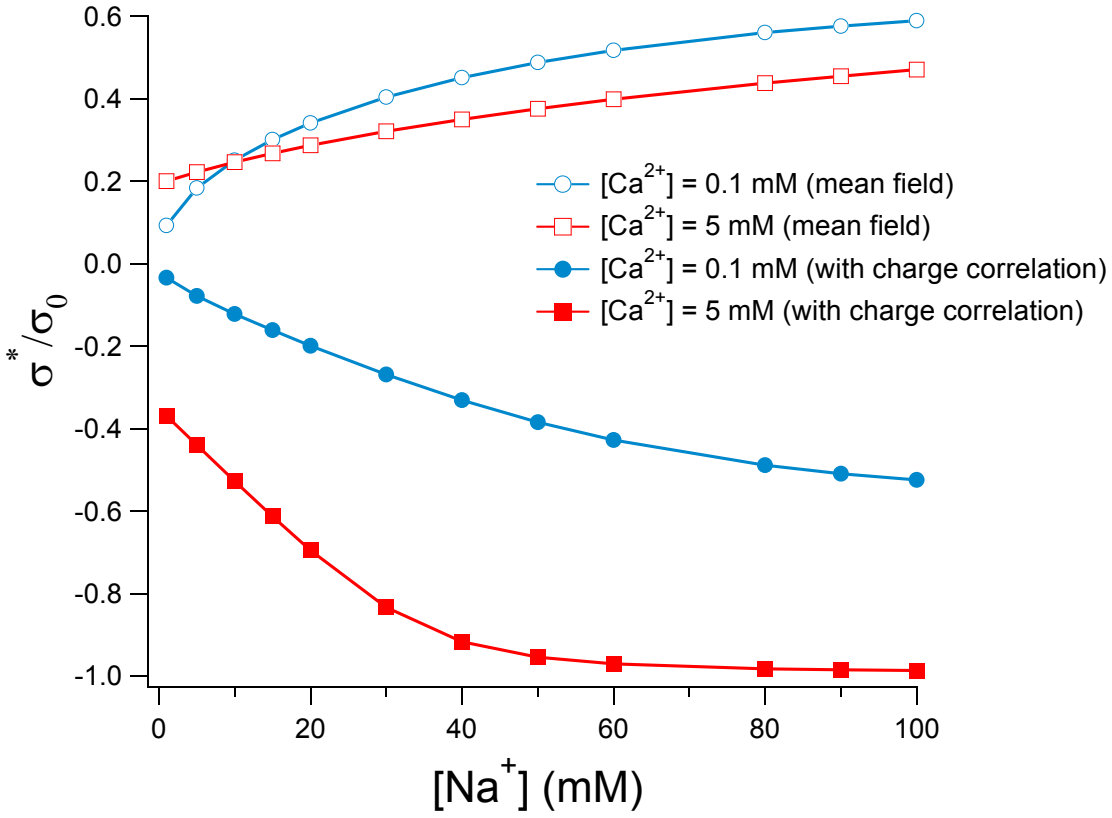

Figure 3.2: Normalized effective planar density, σ^*/σ_0, of the membrane as a function of bulk salt molar concentration. Unfilled points represent mean-field data and filled points represent data acquired by adding the transverse charge correlation. The gap sizes between monovalent (divalent ions) and surface backbone charges are chosen to be $\delta_{Na} = 0.95$Å and $\delta_{Ca} = 0.99$Å, respectively. The surface is assumed fully charged, $\sigma_0 = -(1/65)$Å^{-2}. Complete reversal takes place at large Na_+ concentrations

divalent ions. For example, even for a small salt concentration of 0.1 mM of Ca^{2+}, the sign of the surface changes. The effect of charge inversion, however, is more pronounced when the bulk concentration of Ca^{2+} increases in the Ca^{2+} concentration range shown.

3.3.2 Comparing binding affinities of Mg^{2+} and Ca^{2+} ions

Divalent cations play key roles in many biological systems. For example, many studies suggest that divalent cations are crucial in the neutralization and bridging of anionic charges of the lipid membranes. Through these processes, they affect the lateral interactions between anionic lipids as well as the stability, fluidity, and melting behaviour of the bilayer. It has also been shown that the lateral interaction between LPS molecules is significantly stronger than that between simple phospolipids [27].

Experimental results show that Ca^{2+} ions are significantly more effective in binding onto the membranes, and therefore have stronger binding affinities than Mg^{2+} ions do. Experimental data shows that Ca^{2+} can have a binding constant that is a ten-times greater than Mg^{2+} [25, 6]. As a result, in the presence of both ions in a solution, Ca^{2+} can win the binding competition against Mg^{2+} even when the concentration of Ca^{2+} is lower than that of Mg^{2+}.

In this section, we investigate the binding affinities of Mg^{2+} and Ca^{2+}. For simplicity, we assume that the two species of divalent cations are identical except for their hydration and bare radii. In our model, we assume the size of ions in the bulk is equal to their hydration radius. We also assume that the gap size between condensed Ca^{2+} ions and their binding sites is equal to their bare radius size because upon its binding, Ca^{2+} can completely lose its surrounding water molecules. This is not, however, the case for Mg^{2+} because Magnesium ions are quite small, and therefore, the hydration shell around them is quite strong. As a result, upon binding to a binding site, Mg^{2+} loses its surrounding water molecules partially. Based on the argument presented in the section 3.2.2 about acceptable values for ion radii, we assume that Calcium Ca^{2+} is a divalent ion with bare radius of 0.99Å and hydration radius of 4.1Å, Magnesium Mg^{2+} is a divalent ion with radius of 1.5Å upon binding to its binding site and hydration radius of 4.3Å, and Sodium Na^{+} is a monovalent ion with radius of 0.95Å upon binding to its binding site and hydration radius of 3.6Å.

Figure 3.3 shows the effective surface charge density of a fully charged membrane as a function of the Na^{+} salt concentration in the solution in presence of either Mg^{2+} or Ca^{2+} ions. We compare the overcharging of the membrane as a result of condensation of Mg^{2+} or Ca^{2+} ions on to it. Overcharging occurs both for Mg^{2+} or Ca^{2+} ions, and as we discussed in the previous section, increasing the bulk concentration of divalent ions makes the overcharging more significant. However, our results show that Ca^{2+} ions are at

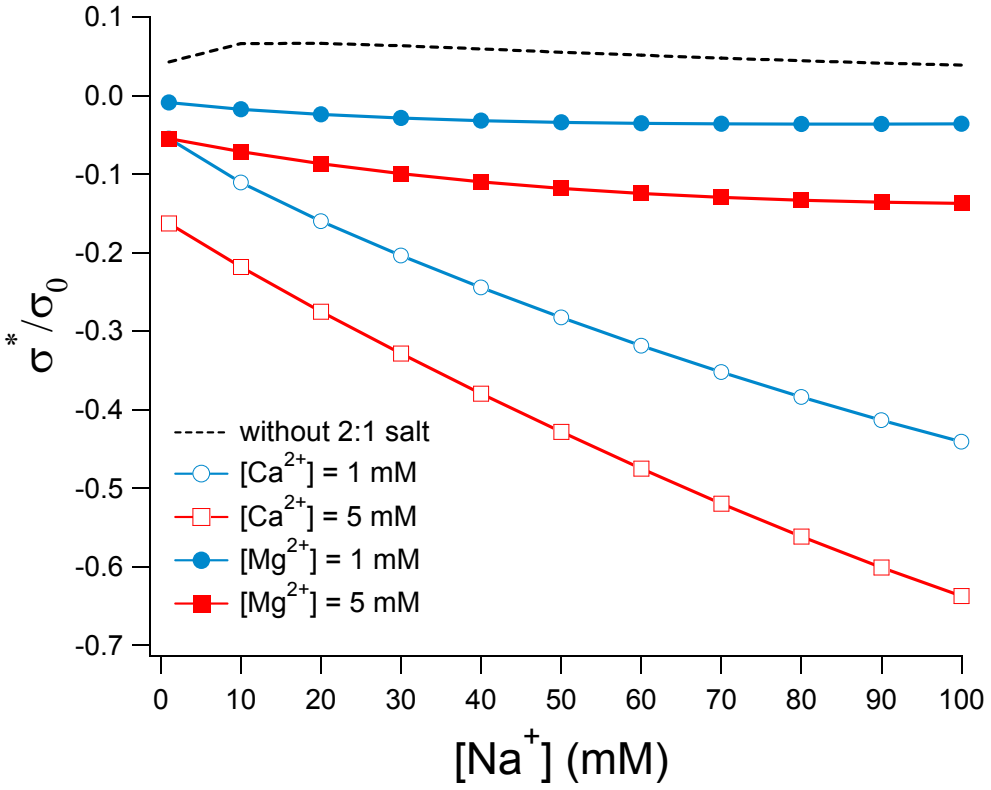

Figure 3.3: Effective surface charge density of a fully charged membrane as a function of the bulk concentration of the monovalent salt in the presence of 1 mM and 5 mM added Mg^{2+} ions (filled points) or Ca^{2+} ions (unfilled points). The value of gap sizes between condensed objects and binding sites are chosen to be $\delta_{Na} = 0.95$Å, $\delta_{Mg} = 1.5$Å, $\delta_{Ca} = 0.99$Å, and their size in bulk is equal to: $R_{Na} = 3.6$Å, $R_{Ca} = 4.1$Å, $R_{Mg} = 4.3$Å.

least six times more successful in binding onto, and therefore, overcharging the membrane compared to Mg^{2+}. Higher condensation of divalent ions on the membrane increases the number of interactions between bound divalent counterions and charged backbone charges. As a result, in line with experimental data, the extra condensation of Ca^{2+} can creates the possibility of effective bridging between anionic lipids by Ca^{2+}, which consequently increases the stability of the lipid bilayer.

Our results suggest that the difference in binding affinities of Mg^{2+} or Ca^{2+} can be attributed to differences of their ion radii in hydration and bare situations. In fact, we could show this characteristic by using only a two-state model for a membrane with discrete charges, which would enable us to take into account the transverse correlations between condensed cations and membrane backbone charges.

3.3.3 Competitive binding between Ca^{2+} and cationic peptide

We compared the binding between Ca^{2+} ions and cationic peptides with negatively charged membranes. Figure 3.4 depicts the normalized charge densities of condensed divalent ions and condensed peptides as a function of the bulk concentration of peptides for different concentrations of salt in solution. It clearly illustrates that adding only a few micromolar of peptides to the solution can result in significant release of Ca^{2+} ions from the membrane's surface. Peptides substitute these released Calcium ions until the number of adsorbed peptides on the surface of the membrane saturates. Figure 3.4 also shows that for higher concentrations of calcium ions in the solution, more divalent ions can remain condensed on the membrane. This is because for higher bulk concentration of divalent ions, the chemical potential of free ions increases, and therefore, more divalent ions have to remain on the surface in order to balance the chemical potential equation.

3.3.4 Summary and Conclusion

In this thesis, we have presented a simple physical model to explain the nature of the competitive binding between divalent counterions and cationic peptides in a simple system where only coulombic and short-range interactions were present. Based on this model, we studied the interactions of cationic antimicrobial peptides with the outer leaflet of Gram-negative bacteria. Using a simple model which allows ions to bind locally to discrete surface charges, we showed that the charge correlations can account for enhanced condensation of counterions on the membrane. We also showed that in line with experimental results, calcium ions are more effective in binding onto lipid membranes compared to magnesium ions.

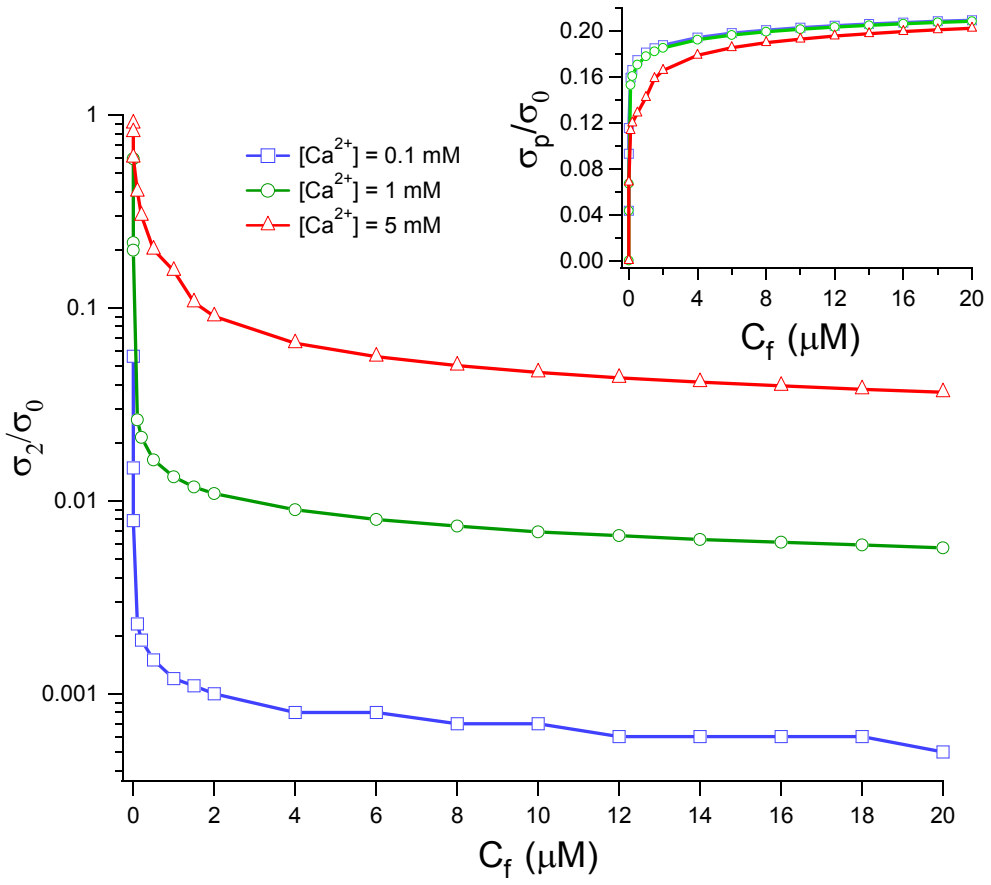

Figure 3.4: Competitive binding between Ca^{2+} ions and peptides. The normalized charge densities of condensed divalent ions and condensed peptides are plotted as a function of free peptide concentration, C_f. The results are compared for different concentrations of Ca^{2+} in bulk.

Finally, our results suggest a physical explanation for the preferred binding of cationic antimicrobial peptides onto the outer leaflet of Gram-negative bacteria. In particular, we showed that even in the presence of a small amount of free peptides in a salty solution, peptides can easily replace the bound divalent ions.

Despite the success of our model in explaining the competitive binding of divalent ions and peptides on a fully charged lipid membrane, other biological details may need to be included in our model as well. Also, a detailed study on the change in the lateral pressure of the membrane seems necessary. Such a study may benefit our endevour in having a better understanding about the destabilization of lipid membranes caused by antimicrobial peptides.

3.4 Appendices

3.4.1 Electrostatic energy of a charged surface

The electrostatic energy of a uniformly planar charged surface in a salty solution can be written as $U = \frac{1}{2}\int \sigma\psi_\perp d^2r$, where $\psi_\perp$ is the potential at the surface and $d^2r = dxdy$. This surface potential in Debye-Hückel limit can be calculated as:

$$\psi_\perp = l_B \int \sigma d^2r \frac{e^{-\kappa|r-r'|}}{|r-r'|} = l_B\sigma \int_0^{2\pi} d\theta \int_0^\infty \rho d\rho \frac{e^{-\kappa\rho}}{\rho} = 2\pi l_B \sigma \kappa^{-1} \tag{3.9}$$

and therefore, the electrostatic energy per unit area of the surface will be $U/A = \pi l_B \sigma^2 \kappa^{-1}$.

3.4.2 M_ν integral in Cartesian coordinates

The integral runs over the regions of $\{|x-x'| < \nu a, |y-y'| < a\}$ over the surface. However, by writing the integral in terms of rotated coordinates, this multiple integral can be simplified to a double integral. In the rotated coordinate $X = |x-x'|, X' = |x+x'|$ (and similarly for y and y' components), the multiple integral which is carried over the whole surface ($x, x', y, y' \in [0, L]$) can be written as:

$$\begin{aligned} M_\nu &= A^{-1} \iint_R d^2r d^2r' \frac{e^{-\kappa|r-r'|}}{|r-r'|} \\ &= A^{-1} \int_0^{\sqrt{2}L} \int_0^{\sqrt{2}L} dX'dY' \int_{-\nu a/\sqrt{2}}^{+\nu a/\sqrt{2}} \int_{-a/\sqrt{2}}^{+a/\sqrt{2}} dXdY \frac{e^{-\kappa\sqrt{X^2+Y^2}}}{\sqrt{X^2+Y^2}} \\ &= 2\int_{-\nu a/\sqrt{2}}^{+\nu a/\sqrt{2}} \int_{-a/\sqrt{2}}^{+a/\sqrt{2}} dXdY \frac{e^{-\kappa\sqrt{X^2+Y^2}}}{\sqrt{X^2+Y^2}} \end{aligned} \tag{3.10}$$

in which A^{-1} cancels out the term L^2 calculated from the first two integrations. The Jacobian of the coordinate rotation is 1 and the limits of simplified integral are chosen so that the integration is over the same surface as the original one. In the limit of $a \ll L$, we can ignore the edge effects and choose the upper limits of X' and Y' to be of order $\sqrt{2}L$.

3.4.3 Entropy of condensed multivalent counterions

The entropic part of the free energy comes from two places: the demixing entropy of counterions bound onto the sites, and the entropy of free counterions. Using the entropy definition, $S = k_B \ln W$ (where W is the number of spatial arrangements of bound ions

on the surface), the demixing entropy of N_ν bound counterions on N_s binding sites in the discrete limit can be written as,

$$\frac{S_{mix}}{k_B} = \ln\left(\frac{N_s!}{N_\nu!(N_s-N_\nu)!}\right) \simeq -\left[N_\nu \ln\left(\frac{N_\nu}{N_s}\right) + (N_s - N_\nu)\ln\left(1-\frac{N_\nu}{N_s}\right)\right]$$

$$\Rightarrow \quad \frac{S_{mix}}{k_B A} = -\left[\sigma_\nu \ln\left(\frac{\sigma_\nu}{\sigma_0}\right) + (\sigma_0 - \sigma_\nu)\ln\left(1-\frac{\sigma_\nu}{\sigma_0}\right)\right] \tag{3.11}$$

where, in the second step, we used Stirling's approximation. We can extend Equation 3.11 for two species of bound counterions N_1 and N_2. The bulk entropy of free counterions, however, is $N_\nu \ln(n_\nu v_0)$, where v_0 is the volume of free counterions. Adding the change in the entropy of monovalent and divalent counterions in the free and bound states, the total entropy of the system in the continuum limit is

$$\begin{aligned} -\frac{\Delta S}{k_B A} &= \sum_{i=1}^{2} \sigma_i \ln\left(\frac{\sigma_i}{\sigma_0}\right) + (\sigma_0 - \sigma_1 - \sigma_2)\ln\left(1-\frac{\sigma_1}{\sigma_0}-\frac{\sigma_2}{\sigma_0}\right) \\ &+ \sum_{i=1}^{2} \sigma_i \ln(n_i v_0) - \sum_{i=1}^{2} n_i \ln(n_i v_0) \end{aligned} \tag{3.12}$$

APPENDICES

Appendix A

Computational Codes

A.1 COMSOL script

Here is a COMSOL Physics code for a disk peptide and a thick sheet membrane. The membrane is demixable, and the peptide and membrane are in aqueous solution that contains the counterions and added monovalent 1:1 salt solution.

```
flclear 'all'

for Q =  4                    % peptide's charge
for alb = [0.05 0.3 0.99]        % ᾱ = average fraction of charged lipids
for CellRadius = [15 15.5 16 16.5 17.5 18.5 20 22.5 25 ...
            30 40 50 60 70 80 90];      % radius of WSC

    dist_pept0 = 100;
    Z = 1;                              % valency of salt ions
    kappa = 0.1;                        % κ = 0.1Å^-1
    a0 = 65;                            % lipid headgroup area
    PepRadius = 10;
    PepThick = 4;
    MembThick = 40;

    epsilon = 0.00014286734768885409;
    lB = 1/(4*pi*80*epsilon);                % l_B = 6.9Å

    coe1 = -0.318173;
    coe2 = -0.318170;

    clear fem;
    sol = 0;
```

```
24
25 % FEM Constants ================================================
26     fem.const.Q = Q;
27     fem.const.Z = Z;
28     fem.const.alb = alb;
29     fem.const.a0 = a0;
30     fem.const.lB = lB;
31     fem.const.kappa = kappa;
32     fem.const.coe = coe1;
33     fem.const.n0 = 'kappa^2/(4*pi*lB*Z*(1+Z))'; %n_0 = 5.8 × 10^-5 Å^-3 ~ 95mM
34     fem.const.PepRadius = PepRadius;
35     fem.const.PepThick = PepThick;
36     fem.const.rhoPept = 'Q/(pi*PepRadius^2 * PepThick)';     % ρ_peptide
37     fem.expr.epsilon = epsilon;
38
39     fem.expr.L = 'coe';
40     fem.expr.al_CON = '(1-alb)/(alb)';
41 %   fem.expr.al = 'alb';                                % No demixing
42     fem.expr.al = 'exp(V-L)/( al_CON+exp(V-L) )';       % with demixing
43     fem.expr.sigmaMemb = 'al/a0';
44
45     fem.expr.np = '1*n0*exp(-Z*V)';
46     fem.expr.nm = 'Z*n0*exp(+1*V)';
47
48 % Geometry ========================================================
49     % WSC as a aqueous medium
50     g2=rect2(CellRadius,'200','base','corner', ...
51           'pos',{'0','-50'},'rot','0');
52     % membrane
53     g3=rect2(CellRadius, MembThick,'base','corner', ...
54           'pos',[0,-MembThick],'rot','0');
55     % Polar sec. of peptide
56     g4=rect2(PepRadius, PepThick,'base','corner', ...
57           'pos',[0, dist_pept0],'rot','0');
58     % Hydrophobic sec. of pept.
59     g5=rect2(PepRadius, PepThick,'base','corner', ....
60           'pos',[0, dist_pept0+PepThick],'rot','0');
61     clear s
62     s.objs={g2,g3,g4,g5};
63     s.name={'Envir','Memb','Polar','Hydrophobic'};
64     s.tags={'g2','g3','g4','g5'};
65
66     fem.draw=struct('s',s);
67     fem.geom=geomcsg(fem);
68     fem.mesh=meshinit(fem, 'hauto',5);
69
70 % Application values ==============================================
71     clear appl
```

```
72      appl.mode.class = 'Electrostatics';
73      appl.mode.type = 'axi';
74      appl.border = 'on';
75      appl.assignsuffix = '_es';
76      clear bnd
77      bnd.rhos = {0,0,0,'-sigmaMemb',0};
78      bnd.type = {'V0','cont','ax','r','D'};
79      bnd.ind = [3,1,3,2,3,4,3,2,3,2,3,2,1,2,2,5,5,5];
80      appl.bnd = bnd;
81      clear equ
82      equ.epsilonr = {80,2,40,3};
83      equ.rho = {'-kappa^2*(exp(V)-exp(-Z*V))/(1+Z)*epsilon0_es*epsilonr_es', ...
84                 0,'rhoPept',0};
85      equ.ind = [1,2,1,3,4];
86      appl.equ = equ;
87      appl.var = {'epsilon0','0.0001428673476885409'};
88      fem.appl{1} = appl;
89      fem.sdim = {'r','z'};
90      fem.frame = {'ref'};
91      fem.border = 1;
92
93  % Loop for moving peptide ========================================
94  dist_pept = dist_pept0;
95
96  for pept_displace = [0 -10 -10 -10 -10 -10 -10 -10 -5 -5 -3 -2 -2 ...
97                  -1 -1 -1 -1 -1 -1 -1 -1 -1 -1 -1 -1]
98
99      dist_pept = dist_pept + pept_displace;
100
101     clear s
102     g4 = move(g4, 0, pept_displace);
103     g5 = move(g5, 0, pept_displace);
104     s.objs={g2,g3,g4,g5};
105     s.name={'Envir','Memb','Polar','Hydrophobic'};
106     s.tags={'g2','g3','g4','g5'};
107
108     fem.draw=struct('s',s);
109     fem.geom=geomcsg(fem);
110
111     fem.mesh=meshinit(fem, 'hauto',5);
112     fem=multiphysics(fem);
113     fem.xmesh=meshextend(fem);
114
115 % Solving with a non-demixable membrane ==========================
116     fem=adaption(fem, 'solcomp',{'V'}, 'outcomp',{'V'}, 'nonlin','on', ...
117             'solver','stationary', 'l2scale',[1], 'l2staborder',[2], ...
118             'eigselect',[1], 'maxt',10000000, 'ngen',2, 'resorder',[0], ...
119             'rmethod','longest', 'tppar',1.7, 'geomnum',1);
```

```
120
121 % Solving with a demixable membrane ================================
122     ratio1 = postint(fem,'al*2*r','dl',[6],'edim',1)/(CellRadius^2);
123
124     while abs(ratio1 - alb) > 0.00005
125         fem.const.coe = coe2;
126         fem.sol = femstatic(fem,'init',fem.sol,'solcomp',{'V'}, ...
127                                 'outcomp',{'V'}, 'nonlin','on');
128
129         ratio2 = postint(fem,'al*2*r','dl',[6],'edim',1)/(CellRadius^2);
130
131         coe3 =  (coe2-coe1) / (ratio1-ratio2) * (ratio1-alb) + coe1;
132         if abs(ratio1-alb) > abs(ratio2-alb)
133               coe1 = coe2; ratio1 = ratio2;  coe2 = coe3;
134         else
135         coe2 = coe3;
136         end % end of if
137     end % end of while
138
139     postplot(fem, 'tridata',{'V','cont','internal'}, ...
140                   'trimap','jet(1024)', ...
141                   'title','Surface: Electric potential', ...
142                   'axis',[-173.5,233.5,-112.5,162.5,-1,1]);
143
144 % Calculating Free Energy terms ===================================
145     Eng_salt = postint(fem,'0.5*(np-nm)*V*2*r','dl',[1,3],'edim',2)*pi;
146     Eng_pept = postint(fem,'0.5*rhoPept*V*2*r','dl',[4],'edim',2)*pi;
147     Eng_memb = postint(fem,'-0.5*sigmaMemb*V*2*r','dl',[6],'edim',1)*pi;
148     Eng = Eng_salt + Eng_memb + Eng_pept;
149
150     Ent_V = postint(fem,'((nm-Z*np)*V+nm*log(Z)-(np+nm-2*n0))*2*r', ...
151                         'dl',[1,3], 'edim',2)*pi;
152     Ent_S = 0;
153
154     Lagrange = 0;
155     Free_energ = Eng + Ent_V + Ent_S + Lagrange;
156     [VProf] = postinterp(fem, 'V', [0.1; 0.1]);
157
158 % Integrating counterions and anionic lipids ==========================
159
160     total_Np = postint(fem,'np*2*r','dl',[1,3],'edim',2)*pi;
161     total_Nm = postint(fem,'nm*2*r','dl',[1,3],'edim',2)*pi;
162
163     conf_p_space = postint(fem,'(np-n0)*2*r','dl',[1,3],'edim',2)*pi;
164     conf_m_space =  postint(fem,'(nm-n0)*2*r','dl',[1,3],'edim',2)*pi;
165     totalCharge =  postint(fem,'(np-nm)*2*r','dl',[1,3],'edim',2) * pi;
166
167     fprintf('\n%g %g %g %g %g %g %g %g %g %g %g
```

```
                %g %g %g %g %g %g %g %g %g', ...
        kappa, Q, alb, CellRadius, Z, ...
        dist_pept, Eng_salt, Eng_memb, Eng_pept, Eng, Ent_V, Ent_S, ...
        Lagrange,  Free_energ, ...
        total_Np, total_Nm, conf_p_space, conf_m_space, ...
        totalCharge, VProf);

end;

end;end;end;
```

A.2 MATLAB code

Here is a MATLAB code for a competitive binding between a cationic peptide and divalent ions.

```
clear;clc; warning off;

a = 8.0623;     % corresponding to σ = 1/65
s0 = 1/a^2;
lB = 7.1;

n1 = 1e-3*[100];
n2 = 1e-3*[1 2 4];
np = 1e-6*[.1 .2 .4 .6 .8 1 1.5 2 4 6 8 10 12 14 16 18 20];
conv = 6.022*1e-4;
% conversion factor from Molar to inverse Angstrom cube, = N_A/(1L * 10^27 A^3)

dlt1 = 2;                   dlt2 = 1.5;                 dltp = 2.3;
Z1 = 1;                     Z2 = 2;                      Zp = 4;
v01 = 4/3*pi*(3.6)^3;       v02 = 4/3*pi*(4.1)^3;        v0p = 2500;

for i = 1:size(n1,2)
for j = 1:size(n2,2)
for k = 1:size(np,2)
    kappa = sqrt( 4*pi*lB*(2*n1(i)*conv + Z2*(Z2+1)*n2(j)*conv) );
    dlim = a/sqrt(2);
    F = @(x,y) exp( -kappa.*sqrt(x.^2+y.^2) ) ./ sqrt(x.^2+y.^2);
    M1 =  8*dblquad(F,0,Z1*dlim, 0,dlim);
    Mp =  8*dblquad(F,0,Zp*dlim, 0,dlim);

    c1 = -2*pi*lB*kappa^(-1);

    b1 = c1*Z1*s0 +lB*M1*s0*Z1 -lB/dlt1*Z1 - log(n1(i)*conv*v01);
```

```
29      b2 = c1*Z2*s0 +lB*M1*s0*Z2 -lB/dlt2*Z2 - log(n2(j)*conv*v02);
30      bp = c1*Zp*s0 +lB*Mp*s0    -lB/dltp*Zp - log(np(k)*conv*v0p);
31
32      a11 = (-c1-lB*M1)*Z1*Z1;
33      a21 = (-c1-lB*M1)*Z2*Z1;
34      ap1 = (-c1*Z1-lB*M1)*Zp;
35
36      a12 = (-c1-lB*M1)*Z1*Z2;
37      a22 = (-c1-lB*M1)*Z2*Z2;
38      ap2 = (-c1*Z2-lB*M1)*Zp;
39
40      a1p = (-c1*Z1-lB*M1)*Zp;
41      a2p = (-c1*Z2-lB*M1)*Zp;
42      app = (-c1*Zp*Zp-lB*M1);
43
44      F = @(s) [  b1+a11*s(1,:)+a12*s(2,:)+a1p*s(3,:) + ...
45                      log(s(1,:))-log(s0-s(1,:)-s(2,:)-s(3,:)) ; ...
46                  b2+a21*s(1,:)+a22*s(2,:)+a2p*s(3,:) + ...
47                      log(s(2,:))-log(s0-s(1,:)-s(2,:)-s(3,:)) ; ...
48                  bp+ap1*s(1,:)+ap2*s(2,:)+app*s(3,:) + ...
49                      log(s(3,:))-log(s0-s(1,:)-s(2,:)-s(3,:)) ];
50      options = optimset('Display', 'final', ...
51              'TolFun', 1e-9, ...
52              'TolX', 1e-9, ...
53              'MaxFunEvals', 1e5, ...
54              'MaxIter', 200);
55      [sig(:,i,j,k), fval] = fsolve(F,[0.0001;0.00001;0.0001], options);
56  end % for i
57  end % for j
58  end % for k
59
60  %=============== PLOT FIGURES ===============
61  figure;
62  t(:,:) = sig(2,1,:,:);
63  gca1 = plot(np*1e6, t(:,:)./s0, '-o');
64  xlabel('{\fontsize{14} C_f (\mu M)}');
65  ylabel('{\fontsize{14} \sigma_2/\sigma_0}');
```

Bibliography

[1] Bruce Alberts, Alexander Johnson, Julian Lewis, Martin Raff, Keith Roberts, and Peter Walter. *Molecular Biology of the Cell, fourth edition*. Garland Science, 2002. 1, 3, 4, 35

[2] Dan Ben-Yaakov, Yoram Burak, David Andelman, and Samuel A. Safran. Electrostatic interactions of asymmetrically charged membranes. *Europhysics Letters*, 79:48002, 2007. 10, 18

[3] Koen Besteman, Marcel A. G. Zevenbergen, Hendrik A. Heering, and Serge G. Lemay. Direct observation of charge inversion by multivalent ions as a universal electrostatic phenomenon. *Phys. Rev. Lett.*, 93(17):170802, 2004. 42, 43

[4] David Boal. *Mechanics of the Cell*. Cambridge University Press, 2002.

[5] Kim A. Brogden. Antimicrobial peptides: pore formers or metabolic inhibitors in bacteria? *Nature Reviews Microbiology*, 3(3):238–250, 2005. 3

[6] Jeffrey W. Smith Dana D. Hu, John R. Hoyer. Ca^{2+} suppresses cell adhesion to osteopontin by attenuating binding affinity for integrin $\alpha_v\beta_3$. *The Journal of Biological Chemistry*, 1995. 45

[7] Margitta Dathe and Torsten Wieprecht. Structural features of helical antimicrobial peptides: their potential to modulate activity on model membranes and biological cells. *Biochimica et Biophysica Acta*, 1462:71–87, 1999. 3

[8] Margitta Dathe, Torsten Wieprecht, and et al. Hydrophobicity, hydrophobic moment and angle subtended by charged residues modulate antibacterial and haemolytic activity of amphipathic helical peptides. *FEBS Letters*, 403:208–212, 1997. 3

[9] Ilia G. Denisov, Steve Wanaski, and et al. Binding of basic peptides to membranes produces lateral domains enriched in the acidic lipids phosphatidylserine and phosphatidylinositol 4,5-bisphosphate: An electrostatic model and experimental results. *Biophysical Journal*, 74(2):731–744, 1998. 25

[10] Richard M. Epand and Hans J. Vogel. Diversity of antimicrobial peptides and their mechanisms of action. *Biochimica et Biophysica Acta*, 1462(11-28), 1999. 5, 35

[11] Jordi Faraudo and Alex Travesset. The many origins of charge inversion in electrolyte solutions: Effects of discrete interfacial charges. *J. Phys. Chem. C*, 111(2):987994, 2007. 37, 42

[12] William M. Gelbart, Robijn F. Bruinsma, Philip A. Pincus, and V. Adrian Parsegian. DNA-inspired electrostatics. *Physics Today*, 53(9):38–44, 2000. 10, 14, 23, 32

[13] Bae-Yeun Ha. Stabilization and destabilization of cell membranes by multivalent ions. *Phys. Rev. E*, 64(5):051902, 2001. 35

[14] Bae-Yeun Ha. Effect of divalent counterions on asymmetrically charged lipid bilayers. *Phys. Rev. E*, 67(3):030901, 2003. 35

[15] Thomas Heimburg, Brigitta Angerstein, and Derek Marsh. Binding of peripheral proteins to mixed lipid membranes: Effect of lipid demixing upon binding. *Biophysical Journal*, 76:25752586, 1999. 27

[16] Mark L. Henle, Christian D. Santangelo, Deena M. Patel, and Philip A. Pincus. Distribution of counterions near discretely charged planes and rods. *Europhysics Letters*, 66:284, 2004. 36

[17] Jacob N. Israelachvili. *Intermolecular and Surface Forces, Second Edition*. Academic Press, 1992. 42

[18] Ziqing Jiang, Adriana I. Vasil, and et al. Effects of net charge and the number of positively charged residues on the biological activity of amphipathic -helical cationic antimicrobial peptides. *Biopolymers (Peptide Science)*, 90(3):369–383, 2007. 3, 12

[19] Lakshmi P. Kotra, Dasantila Golemi, and et al. Dynamics of the lipopolysaccharide assembly on the surface of escherichia coli. *J. Am. Chem. Soc.*, 121(38):87078711, 1999. 5

[20] Ellen Kuchinka and Joachim Seelig. Interaction of melittin with phosphatidylcholine membranes. binding isotherm and lipid head-group conformation. *Biochemistry*, 28:42164221, 1989. 25

[21] Katsumi Matsuzaki. Why and how are peptide-lipid interactions utilized for self-defense? magainins and tachyplesins as archetypes. *Biochimica et Biophysica Acta (BBA) - Biomembranes*, 1462(1-2):1–10, 1999. 3

[22] Sylvio May, Daniel Harries, and Avinoam Ben-Shaul. Lipid demixing+ and protein-protein interactions in the adsorption of charged proteins on mixed membranes. *Biophysical Journal*, 79(4):1747–1760, 2000. 10, 12, 13, 25

[23] Donald A. McQuarrie. *Statistical mechanics*. University Science Books, 2000. 6

[24] Philip Nelson. *Biological Physics: Energy, Information, Life*. W. H. Freeman, 2003. 14, 32

[25] Carolyn Newton, Walter Pangborn, Shlomo Nir, and Demetrios Papahadjopoulos. Specificity of ca^{2+} and mg^{2+} binding to phosphatidylserine vesicles and resultant phase changes of bilayer membrane structure. *Biochimica et Biophysica Acta (BBA) - Biomembranes*, 506(2):281 – 287, 1978. 45

[26] Toan T. Nguyen, Alexander Yu. Grosberg, and Boris I. Shklovskii. Macroions in salty water with multivalent ions: Giant inversion of charge. *Phys. Rev. Lett.*, 85(7):1568–1571, 2000. 35, 42, 43

[27] Hiroshi Nikaido. Molecular basis of bacterial outer membrane permeability revisited. *Microbiology and Molecular Biology Reviews*, 67(4):593+, 2003. 4, 35, 41, 45

[28] Stefan Obst, Manfred Kastowsky, and Hans Bradaczek. Molecular dynamics simulations of six different fully hydrated monomeric conformers of *Escherichia coli* re-lipopolysaccharide in the presence and absence of ca^{2+}. *Biophysical Journal*, 72:1031–1046, 1997. 41

[29] V. Adrian Parsegian and David Gingell. On the electrostatic interaction across a salt solution between two bodies bearing unequal charges. *Biophysical Journal*, 12(9):1192–1204, 1972. 10

[30] Wilson C. K. Poon and David Andelman. *Soft Condensed Matter Physics in Molecular and Cell Biology*. Taylor & Francis, 2006. 6

[31] Sattar Taheri-Araghi and Bae-Yeun Ha1. Physical basis for membrane-charge selectivity of cationic antimicrobial peptides. *Phys. Rev. Lett.*, 98(16):168101, 2007. 10, 12, 13

[32] Alex Travesset and David Vaknin. Bjerrum pairing correlations at charged interfaces. *Europhysics Letters*, 74:181, 2006. 35

[33] Esov S. Velazquez and Lesser Blum. Electrolytes confined to a plane in the debye-huckel theroy. *Physica A*, 244:453–460, 1997. 28

[34] Torsten Wieprecht, Margitta Dathe, and et al. Influence of the angle subtended by the positively charged helix face on the membrane activity of amphipathic, antibacterial peptides. *Biochemistry*, 36(42):1286912880, 1997. 3

[35] Michael Zasloff. Antimicrobial peptides of multicellular organisms. *Nature*, 415:389–395, 2002. 3